General Disclaimer

One or more of the Following Statements may affect this Document

- This document has been reproduced from the best copy furnished by the organizational source. It is being released in the interest of making available as much information as possible.

- This document may contain data, which exceeds the sheet parameters. It was furnished in this condition by the organizational source and is the best copy available.

- This document may contain tone-on-tone or color graphs, charts and/or pictures, which have been reproduced in black and white.

- This document is paginated as submitted by the original source.

- Portions of this document are not fully legible due to the historical nature of some of the material. However, it is the best reproduction available from the original submission.

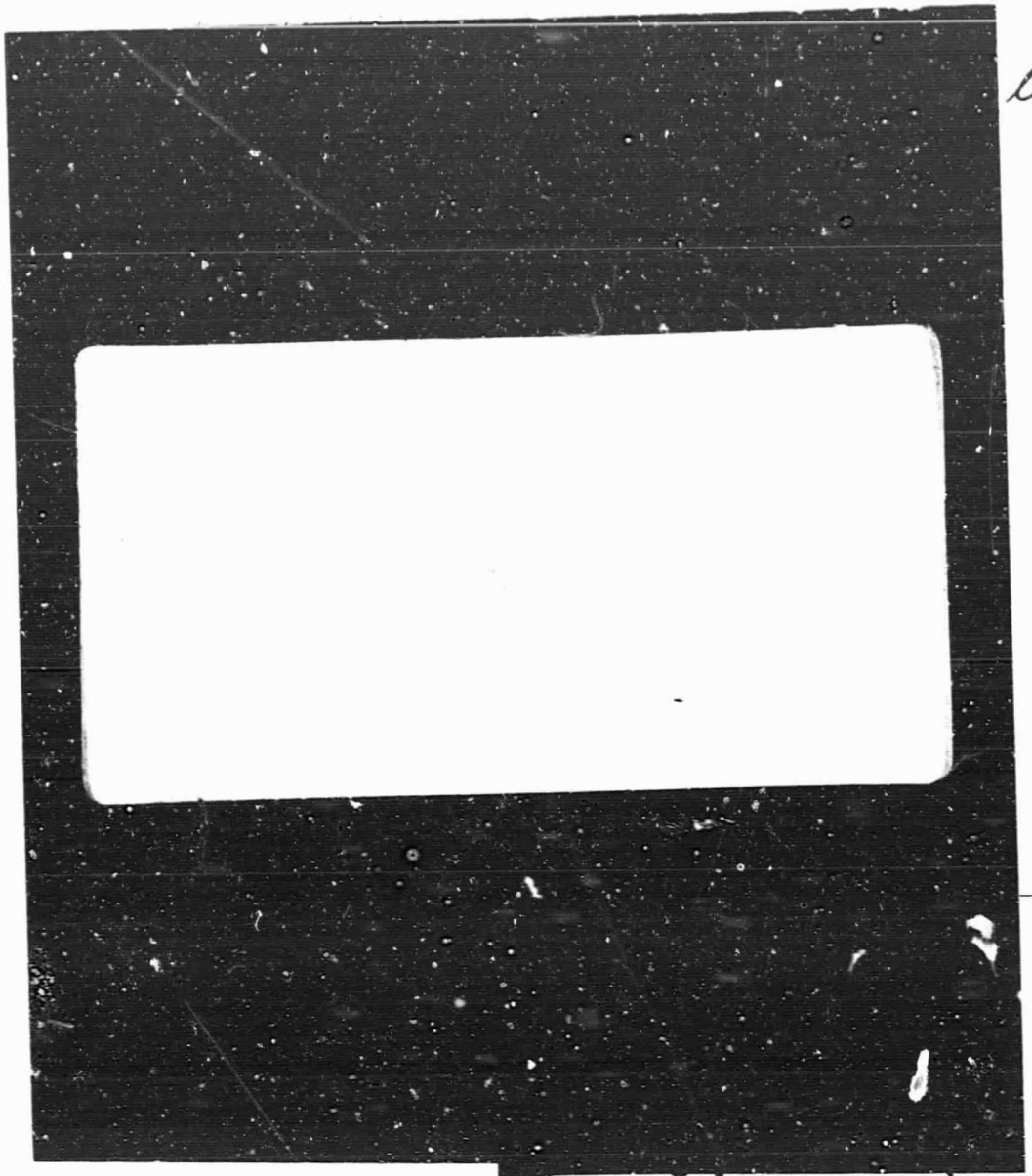

CR-86082

GPO PRICE $ _____

CFSTI PRICE(S) $ _____

Hard copy (HC) 3.00

Microfiche (MF) .65

ff 653 July 65

FACILITY FORM 602

N68-31070 (ACCESSION NUMBER) (THRU)

75 (FAGES) 1 (CODE)

CR-86082 (NASA CR OR TMX OR AD NUMBER) 21 (CATEGORY)

TASC

7 LOWELL AVENUE WINCHESTER, MASS 01890 617 729-8800

AUG 1968

RECEIVED
STI FACILITY
INPUT BRANCH

RQT53135

TR-101-3

DESIGN OF STRAPDOWN GYROSCOPES FOR A DYNAMIC ENVIRONMENT

15 July 1968

Second Semi-Annual Report

by Arthur A. Sutherland, Jr.,
William S. Beebee and Arthur Gelb

Prepared under Contract No. NAS12-508 by

THE ANALYTIC SCIENCES CORPORATION
6 Jacob Way
Reading, Massachusetts 01867

Electronics Research Center
NATIONAL AERONAUTICS AND SPACE ADMINISTRATION
Cambridge, Massachusetts

Dr. Herbert Weinstock
Technical Monitor
NAS 12-508
Electronics Research Center
575 Technology Square
Cambridge, Massachusetts 02139

ABSTRACT

This document summarizes work accomplished over the period December 1967 to May 1968 in a continuing study of strapdown gyroscope design. Three common pulse torquing techniques for strapdown gyros are described. The important considerations in choosing a rebalance scheme are reviewed and the relative advantages of the three approaches are discussed. Compensation of limit cycling binary torqued gyros is treated with the goal of providing a better closed loop response. A discussion of the dithered binary gyro is presented, illustrating limit cycle determination and closed loop characteristics.

The ternary pulse rebalanced gyro is analyzed using describing functions. Closed loop sinusoidal transfer characteristics are obtained and the effect of random signals at the logic input are investigated. A brief discussion of the proposed gyro and system error simulation is presented and attention is given to gimbal misalignments resulting from angular rates about the output axis.

TABLE OF CONTENTS

TABLE OF CONTENTS (Cont.)

1. INTRODUCTION

The single-degree-of-freedom gyro perfected for platform inertial guidance systems can exhibit large errors when adapted to the strapdown application. The major new error sources are angular motion of the sensor and the rebalance torque loop required to null the gimbal output angle. This report documents some aspects of work performed in a continuing study of strapdown gyroscope design.

Prior work is reported in Refs. 1 and 2. These two documents provide a comprehensive review of important error sources in strapdown single-degree-of-freedom gyros. Different rebalance loop configurations were discussed and their contributions to gyro errors were treated. Particular emphasis was placed on analysis of the limit cycling binary gyro using describing functions. A system level figure-of-merit was established relating gyro errors to system attitude error growth. The optimum set of gyro parameters, those which minimize system error at some point in time, were determined by analytic means. In the references it was concluded that, under the assumptions used in the analysis, gyro parameter manipulation alone cannot reduce strapdown gyro induced errors to a satisfactory level. Several schemes for additional compensation of strapdown gyro errors were proposed and analyzed. Most of them involve the use of additional motion sensors and application of corrections to the gyro. The work presented in these two documents introduced seldom used techniques for analysis of strapdown gyros.

The effort discussed in this report continues that analysis. Three basic pulse rebalance techniques are described. Important considerations in selecting a torquing scheme are discussed and the relative merits of the

three approaches are reviewed. The ternary torqued gyro is treated using describing function theory and time modulated two level torquing is analyzed. Motivation is presented for the construction of a comprehensive strapdown gyro simulation which evaluates system attitude errors. In addition, gimbal suspension design is discussed. The appendices provide some details of describing function analysis. It is shown that the ternary gyro loop response is very sensitive to input amplitude and frequency. On the other hand, time modulated torquing permits analysis of the gyro loop using techniques developed for linear systems. This technique may provide satisfactory closed loop performance without requiring loop compensation. One conclusion is that the time modulation pulse torquing scheme deserves serious consideration for use in strapdown gyros.

2. DESCRIPTION OF PULSE TORQUING SCHEMES

2.1 PULSE REBALANCED GYROS

The single-degree-of-freedom pulse rebalanced gyro shown in Figure 2.1-1 generates an angular rotation about its output axis (output angle) which, for small angles, is proportional to the time integral of angular rate about the case-fixed input axis. In platform inertial navigation systems the sensor package is kept at a fixed attitude with respect to a non-rotating set of coordinates by gimbal rotations which null the gyro output angle. When the gyros are mounted on the vehicle structure, as in a strapdown system, it becomes necessary to provide some other means to keep the output angle small. Powerful torque generators are added to counter the gyroscopic moment created about the output axis when angular rates take place about the gyro input axis. The time integral of applied torque then becomes an indication of the net rotation about the input axis. Consequently, the accuracy of the strapdown gyro is limited by our ability to measure torque generator output.

The appropriate indication of torquer output is current flow through the device. An indirect measurement, torquer current is subject to the nonlinearities and uncertainties which relate it to the true object of the measurement — torque applied about the gyro output axis. In order to ensure accuracy and reduce calibration complexity it has become common practice in strapdown gyros to provide current to the torquer at two or three accurately determined levels. Current duration is also carefully specified in advance and the result is an output which is a digital representation of the current-time integral, i.e., of rotation rather than angular rate.

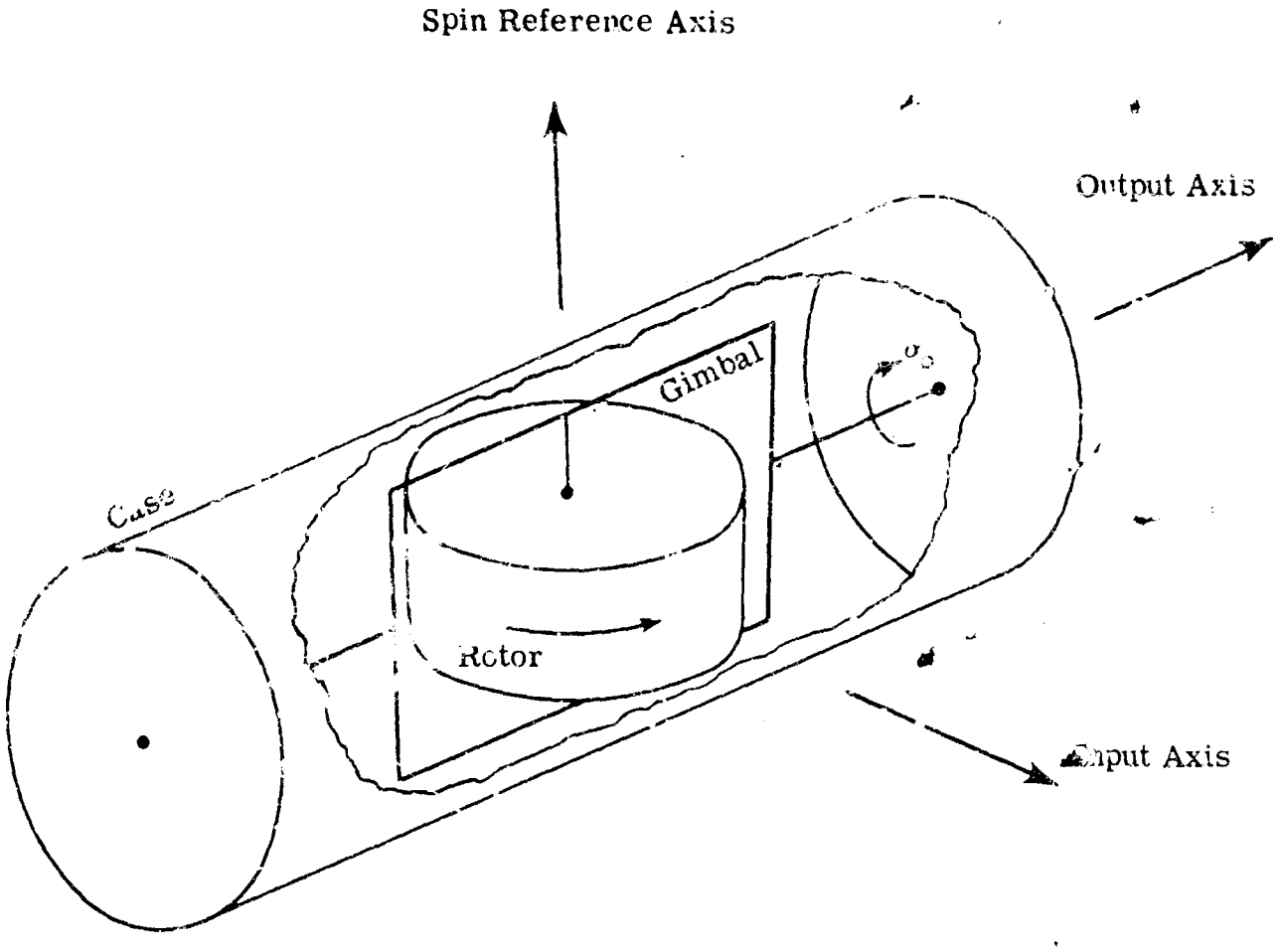

Figure 2.1-1 Single-Degree-of-Freedom Gyro

Binary Delta Modulation — The binary delta modulation pulse torquing scheme provides a torquer current level of fixed magnitude with the same sign as the output angle. Figure 2.1-2 illustrates the binary detection logic used to determine torquer current. The output of this logic is interrogated periodically. Current level may be applied over the entire period or may be dropped to zero after a fixed percent of the interrogation period has passed. The gyro output consists of a single positive or negative count at each interrogation. The net gyro output over any period is computed from the net output count and knowledge

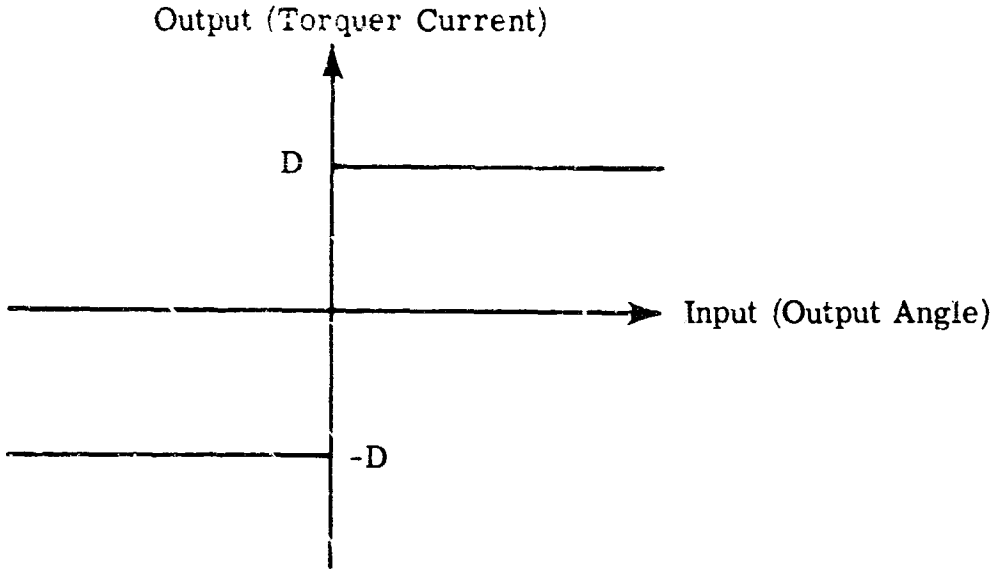

Figure 2.1-2 Two Level Logic

of the incremental angle represented by each accurately metered current pulse. Figure 2.1-3 shows a representative train of torque pulses applied to the gyro. The torque pulse shape differs from that of the current rectangular pulse described above because of torque generator dynamics.

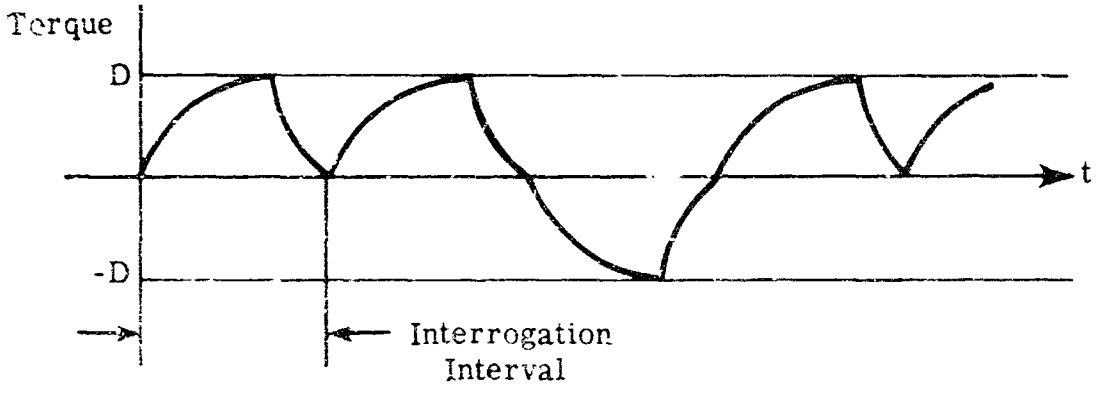

Figure 2.1-3 Representative Torque Output From Delta Modulated Pulse Rebalance Technique

Ternary Delta Modulation — The ternary delta modulation scheme permits the absence of a torque pulse. This can be viewed as an additional (zero) current level. Figure 2.1-4 illustrates the ternary detection logic. The

deadzone 2δ, or region of input which provides no output, is symmetric about zero. For low frequency inputs, δ can be related to an input rotation which will not be detected by the gyro. However, for input frequencies above the float bandwidth, the relation is more complex. The operation of the ternary delta modulation scheme is otherwise identical to the binary technique just discussed.

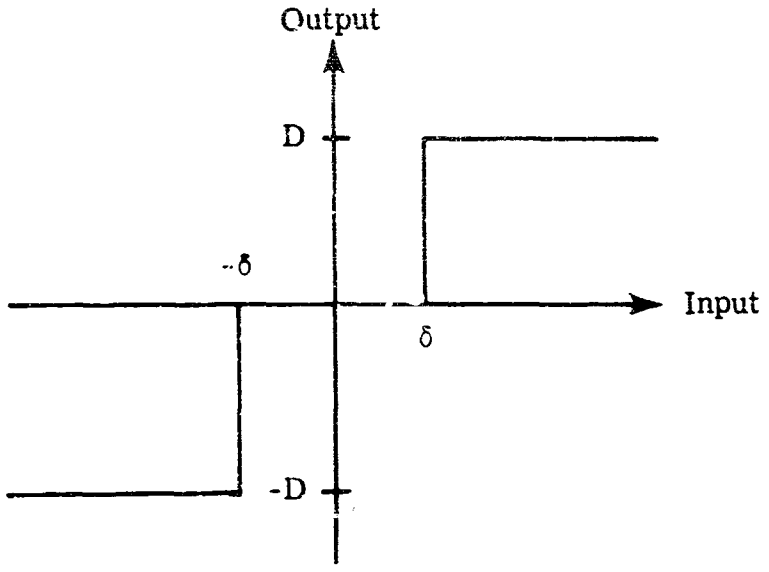

Figure 2.1-4 Three Level Logic

Time Modulation – A third pulse torquing technique, time modulated torquing, adds the gyro output angle to a periodic waveform and employs binary logic on the sum. Figure 2.1-5 illustrates this approach. The net signal is interrogated at a higher frequency than that of the added waveform. In the figure, torquer current changes sign when the sawtooth resets and at the first interrogation point at which the net signal becomes negative. The result is one positive and one negative current pulse each period of the sawtooth, the relative lengths of the two pulses being determined by the gyro output angle (See Figure 2.1-6). Since the periodic waveform is divided into a finite number of equal intervals,

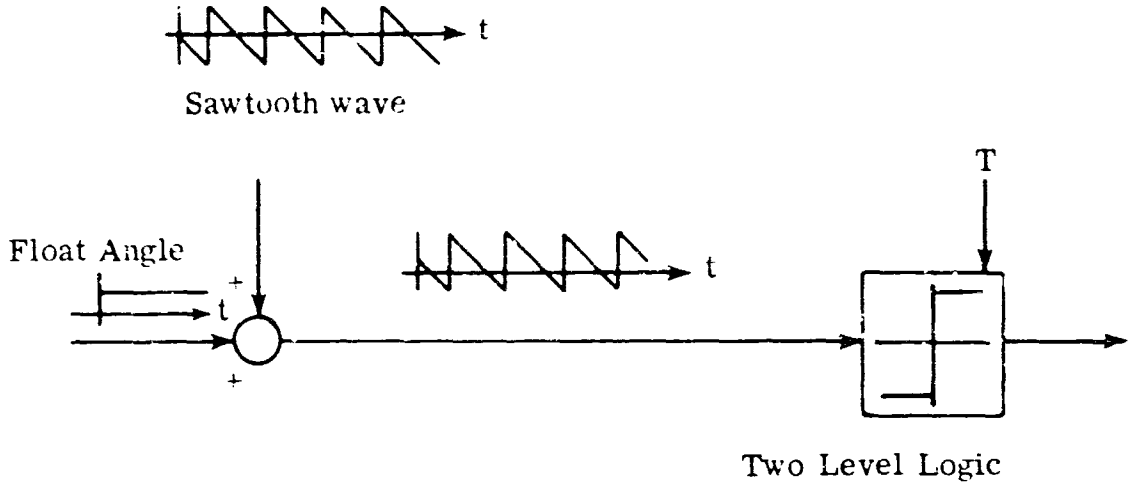

Figure 2.1-5 Time Modulated Torquing

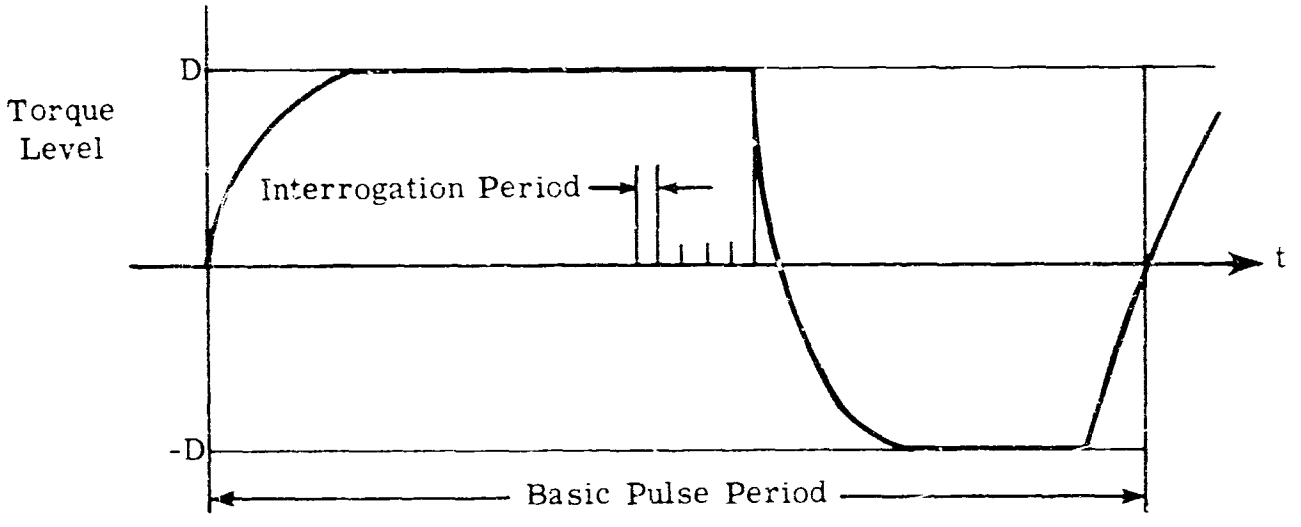

Figure 2.1-6 Torquer Waveform For Time Modulated Torquing

the number of interrogations taking place before the current level switches provides a digital measure of incremental rotation about the gyro input axis.

All three approaches provide digital sensor outputs which represent increments of angular rotation about the sensor input axis. The angular rotation is implied from a carefully calibrated torque pulse applied to the gyro gimbals. Any deviation of the actual time integral of torque from that represented by each output quantum will cause an error in the gyro output which is not recoverable, i.e., differs from gyro output errors caused by storage of information by the float. Constant deviation of the torque pulse can cause constant gyro drift rates while random variations provide random output errors. Differences between the net torque pulses generated and those implied by the rebalanced gyro output are a major source of error in this kind of strapdown sensor.

When system accuracy is considered, factors such as quantization and the information rate of pulse rebalanced gyros are important. The presence of unforced oscillations in the gyro output is also considered when comparing strapdown gyro torquing schemes. In addition, frequency response characteristics and energy dissipation in the gyro loops are important. The major causes and effects of pulse rebalancing errors are described below, followed by a discussion of the weaknesses and strengths of each torquing scheme.

2.2 ASPECTS OF PULSE TORQUING GYRO ERRORS

Torque Pulse Variations — Deviations of the torque pulse size are caused primarily by variations in torquer current level and timing errors in starting and stopping the current flow. Of the two effects, current level errors

are basically independent of the torquing scheme while the system error caused by imperfect switching is related to the frequency with which torque is changed from one level to another. If either current level or switching delay exhibit consistent variations between torque pulses of different signs, Figure 2.4-10 of Ref. 1 can be used to determine the drift rates which result. Random deviations in the switching circuit delay will generate random gyro output errors. Consequently, the rms system attitude error (as reflected in the figure-of-merit described in Ref. 2) will grow as the square root of time. If the timing errors are uncorrelated, rms gyro output error over any period of time is related to the square root of the number of changes in current level which took place. Therefore, gyros that can change current level more frequently have the potential to generate larger system errors by this means. In delta modulated pulse torquing techniques the pulse frequency is directly related to output quantization level and a definite tradeoff exists.

Quantization — The output of pulse rebalanced strapdown gyros is a series of digital pulses each of which represents an incremental rotation about the input axis. This form is not well suited for drift free calculation of the direction cosine matrix because information regarding the order in which rotations take place about the system axes is lost. The commutativity errors which can result are largely related to the gyro output quantization level and the manner and speed with which the outputs are processed. As a general rule, fine quantization is to be preferred. Delta modulated pulse torquing schemes achieve fine quantization by changing the torque level rapidly, thereby allowing very small torque pulses. A practical limitation on the torque pulse size is provided by the torquer time constant. If the desired torque level is changed too frequently the actual torque will not build up to its peak value before changing and torquing efficiency is sacrificed. In the time modulation torquing scheme, quantization is not tied directly to pulse width. The torque switching

frequency is strictly limited and quantization is achieved by specifying the number of points in each cycle at which the torque can make an irreversible sign change. In the absence of switching delays, infinitisimal quantization is possible. The practical limit is imposed by the ability to switch the torque levels accurately in time. Torquer time constant problems are eliminated by restricting the minimum positive or negative pulse lengths in a well designed instrument.

Information Rate — Information rate, defined as the frequency with which new indications of system motion reach the direction cosine computer, varies between the different pulse torquing techniques. Generally, both delta modulation schemes can provide the same maximum information rate, determined by the frequency with which the torque levels can change. The time modulated torquing scheme usually gives new gyro outputs much less frequently (this may also be viewed as a larger delay in transferring information) though with as good or better quantization than the other torquing techniques. The desirability of a high information rate depends on the computer which is used to update the direction cosine matrix. If a Digital Differential Analyzer is used, gyro outputs can be processed as received and the single output level of delta modulated instruments is desirable. On the other hand, if a whole word computer is provided any of the three torquing schemes can generate outputs fast enough to make best use of the computer and the finer quantization available from the time modulated technique is desirable.

Unforced Oscillations — All three pulse torquing schemes produce unforced oscillations in the gyro loop at one time or another. The limit cycle behavior of a control loop containing a binary nonlinearity is well known (see Ref. 1). In the presence of many inputs, the three level pulse torqued gyro will also exhibit wrong way pulses and the time-modulation scheme can give an incorrect net output averaged over each torque cycle. The unwanted

oscillations all result from quantization of the torque-time integral. Limit cycles in pulse rebalanced gyros can result in pseudo-coning system errors if they occur with proper phase and at the same frequency. The binary delta modulation scheme is usually thought to be the least satisfactory from this point of view. However, it can be shown that slight differences between limit cycle periods of the different gyros in a strapdown triad will prevent large system errors of this type (see Ref. 1).

Oscillations of the gyro float can also provide rectified cross-coupling errors. The binary delta modulation technique, with its ever-present limit cycle, and binary time-modulation with its forced float oscillation appear most likely to generate rectified crosscoupling errors.

Gyro Frequency Response Characteristics — One representation of the gyro loop transfer characteristics is the closed loop gain to oscillatory input angular rates at different frequencies. The approximate determination of this characteristic is discussed for the ternary delta modulation and time modulation schemes in this report while analysis of the binary delta modulation technique is presented in Ref. 1. The ternary approach contains one serious disadvantage in this respect; its gain to input signals is very much amplitude dependent. Also, the other two schemes lend themselves much better to manipulation of the frequency response through loop compensation.

Energy Dissipation — Temperature gradients within the gyro structure are a major cause of single-degree-of-freedom gyro drift. If the gradients can be held constant, proper testing will enable accurate compensation of these effects. While it consumes less total power in most motion environments, the ternary delta modulation torquing scheme does not usually provide a uniform energy flow into the torquer. To avoid this obvious cause of varying temperature gradients, a constant current source can be switched into

a dummy load when no torque is called for. However, in this case a considerably larger torquer results.

2.3 COMPARISON OF PULSE TORQUING TECHNIQUES

Binary Delta Modulated Torquing — This approach provides a high information rate, a gyro loop response which is linear with respect to input amplitude and constant temperature gradients in the instrument. Its quantization level in a given application is limited by torquer dynamics. A gyro with this rebalance scheme always limit cycles, thereby consuming electrical power in even the most benign environment, and generating potential cross-coupling rectification and pseudo-coning system errors. The uncompensated gyro loop containing this pulse torquing scheme may not exhibit a satisfactory closed loop frequency response. Section 3.1 of this report explores the use of loop compensation to correct this defect.

Ternary Delta Modulated Torquing — This pulse rebalance scheme can conserve electrical power in a benign environment and has less tendency to limit cycle. The gyro usually has a lower drift rate in the absence of an input. It gives a high information rate suitable for DDA calculations but does not have a linear dynamic input-output relationship. To avoid varying temperature gradients within the sensor, a larger torque producing mechanism is required and potential low power consumption must be sacrificed. The quantization level is limited by the torquer time constant. Section 4 of this report deals with the information transfer characteristics of the ternary delta modulated pulse torqued gyro. The closed loop gain to sinusoidal inputs is shown to be input amplitude sensitive and can assume several possible values in certain input frequency ranges.

Time Modulated Torquing -- Time modulated torquing gives potentially better quantization than is currently possible with the other two schemes but has a necessarily lower information rate. The limit cycle appearing at the output is small but the gimbals will always oscillate and sizeable rectified crosscoupling errors can result. For the same quantization this technique is less sensitive to timing errors in switching. An essentially linear response results. Power consumption is high but temperature gradients are constant. The time modulated torquing scheme is treated in Section 3.2 of this report. It is demonstrated that the uncompensated loop for this gyro can be made to exhibit a more satisfactory closed loop frequency response than an instrument using either delta modulation torquing technique.

None of the pulse torquing techniques discussed offers a clear advantage over the others. If constant energy dissipation and linear response are required at the outset, the three level approach seems to forfeit its greatest advantages. Since the trend appears to be toward whole word computers, adequate output rate and finer quantization appear to give the time-modulation scheme considerable promise for future use.

3. BINARY PULSE REBALANCED GYRO

3.1 COMPENSATION OF THE LIMIT CYCLING LOOP

Introduction – The binary gyro loop limit cycles whether or not a rate signal is present at the input (unless the signal is of high enough amplitude to saturate the loop or suitably shaped to quench the limit cycle). As a consequence of this limit cycling property, the closed loop frequency response to an input signal is largely determined by gyro and torquer time constants and not by easily manipulated electrical gains (see Ref. 1, Section 2.4.3). Specifically, if the loop is linearized using describing function techniques, a response characteristic similar to that of a second-order system results, with natural frequency and damping ratio given by

$$\omega_n = \frac{1}{\tau_f}\sqrt{\frac{\tau_f + \tau_{tg}}{2\tau_{tg}}} \quad \text{rad/sec}$$

and

$$\zeta = \sqrt{\frac{\tau_{tg}}{2(\tau_f + \tau_{tg})}} \tag{3.1-1}$$

respectively. These frequency response characteristics cannot be changed without making hardware modifications to change τ_f and τ_{tg}. In addition, no reasonable choice of τ_f and τ_{tg} can make the damping ratio greater than 1/2. Thus, the frequency response is forced to have a peak near ω_n. Clearly, some frequency sensitive compensation may be desired to remove this peak and, more generally, to permit control of the frequency response characteristics without changing τ_f and τ_{tg}.

Following the analysis used in Ref. 1, we represent the effective gain of the binary nonlinearity to a sinusoidal signal by the Dual Input Describing Function (DIDF), written $N_B(A, B)$. This describing function is the ratio of the amplitude of the signal frequency harmonic at the nonlinearity output to the amplitude, B, of the signal at the nonlinearity input when a sinusoid (limit cycle) of amplitude A is also present at the input. If B is considered small compared to A, a simplified form for $N_B(A, B)$ results:

$$N_B(A, B) \cong N_B(A,0) \qquad B << A$$

$$= \frac{2D}{\pi A} \tag{3.1-2}$$

where D is the drive level of the nonlinearity. Appendix A examines in greater detail the conditions under which this approximation holds.

In attempting to compensate the limit cycling binary loop, we must consider the effect the limit cycle has on the total open loop gain and phase performance as seen by the signal sinusoid. The binary nonlinearity DIDF gain to the limit cycle, written $N_A(A)$, is given by

$$N_A(A) = \frac{4D}{\pi A} \; ; \quad B << A \tag{3.1-3}$$

The complex open loop transfer function of the linear part of the loop is written $H(j\omega)$. The definition of the limit cycle requires that, at the limit cycle frequency, ω_ℓ,

$$H(j\omega_\ell)\, N_A(A) = \underline{1/-180^\circ} \tag{3.1-4}$$

The limit cycle amplitude A and frequency ω_ℓ adapt to maintain this equality regardless of the compensation introduced. From Eqs. (3.1-2) and (3.1-3), it can be seen that

$$N_A(A) \cong 2\, N_B(A, B) \quad ; \quad B << A \tag{3.1-5}$$

Substituting for $N_A(A)$ in Eq. (3.1-4) yields

$$H(j\omega_\ell)\, N_B(A, B) = \frac{1}{2} \; \underline{/-180^\circ} \tag{3.1-6}$$

Here, $H(j\omega_\ell)\, N_B(A, B)$ is the expression for the complex open loop gain as seen by the signal sinusoid. We conclude that, due to the adaptive properties of the limit cycle amplitude and frequency, the open loop gain and phase shift as seen by the signal sinusoid will always be $1/2 \; \underline{/-180^\circ}$ at ω_ℓ. This constraint results in a closed loop signal gain of unity and phase shift of -180° at the limit cycle frequency.

Linear Analysis – The linear analysis technique used to investigate in-loop compensation of binary pulse torqued gyros makes use of the rectangular gain-phase plot (Nichols chart). The open loop gain and phase characteristics are plotted as a function of frequency. On the same plot, lines of constant M(closed loop amplitude ratio) are constructed. The closed loop amplitude ratio for any sinusoidal input is the value of M intersected by the open loop gain-phase curve at the same frequency. The M=1 line represents the desired unity closed loop gain. Figure 3.1-1 shows the M=1 line and the gain-phase curve of the uncompensated gyro loop with the following parameters:

$\tau_{tg} = 10^{-4}$ sec $\qquad K_{sg} = 2\times10^{4}$ mv/rad

$\tau_f = 2.5\times10^{-3}$ sec $\qquad K_{tg} = 1200$ dyne-cm/ma

$C = 10^{5}$ dyne-cm-sec

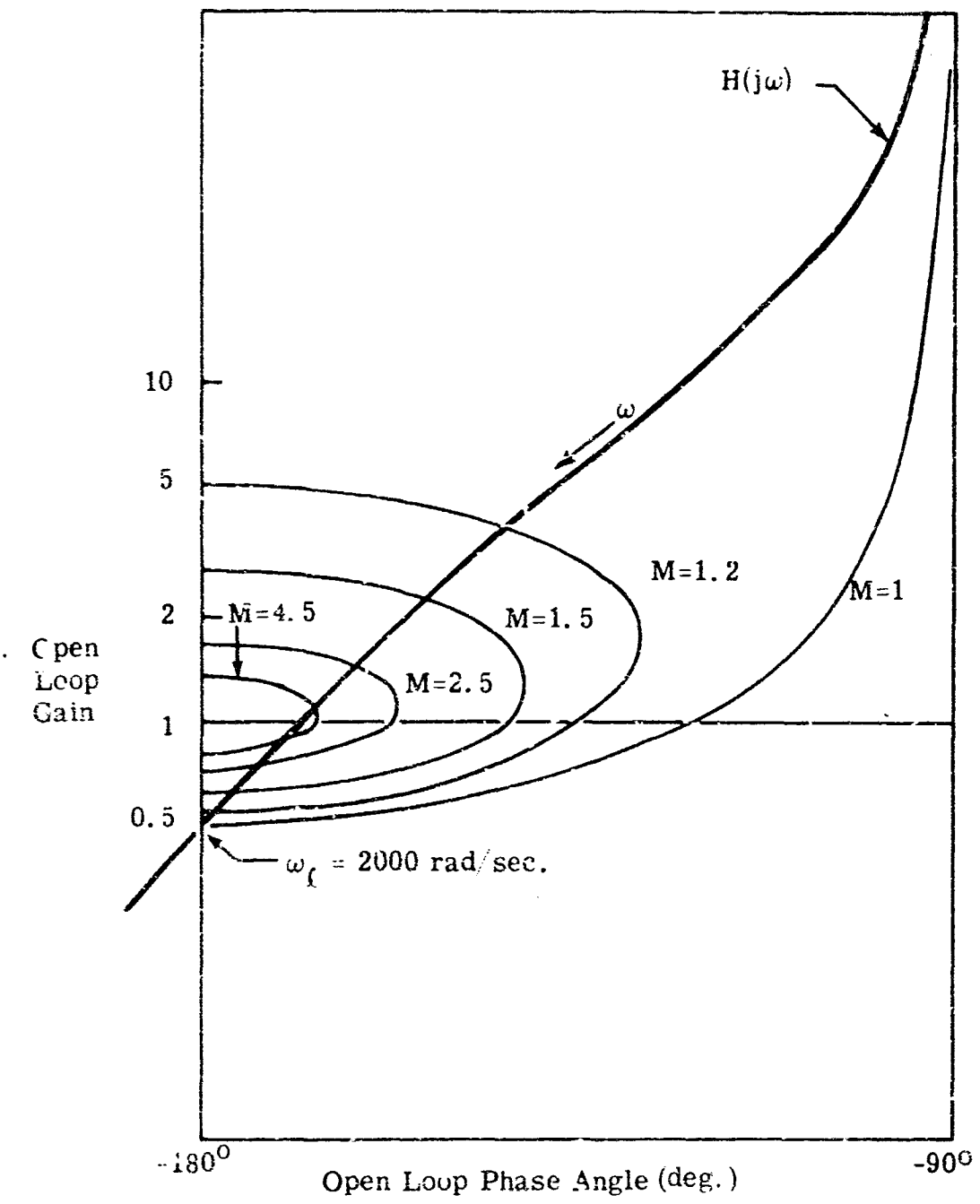

Figure 3.1-1 Open Loop Gain-Phase Plot for Uncompensated Binary Gyro

Note that the gain-phase curve cuts through high closed loop gain lines at frequencies lower than ω_ℓ, producing a peaked frequency response. In order to obtain unity closed loop gain at all frequencies below the limit cycle, we must make gain and phase changes to the open loop which cause the compensated gain-phase curve to coincide with the M = 1 line. As discussed in the previous paragraph, the complex open loop gain must always be $1/2 \angle -180^\circ$ at the limit cycle frequency, ω_ℓ; the gain-phase curve must cross the -180° phase shift line with a gain of 1/2 at ω_ℓ whether or not compensation is used. It can be seen from Fig. 3.1-1 that the M = 1 line also intersects the -180° line at 1/2. Since sinusoidal signals at frequencies beyond ω_ℓ are not of major interest, we will devote our consideration to the frequency range up to and including that of the limit cycle. Four sets of linear dynamic compensation are discussed. In each case the compensation is assumed to be placed in the forward signal path as illustrated in Fig. 3.1-2. The presence of the

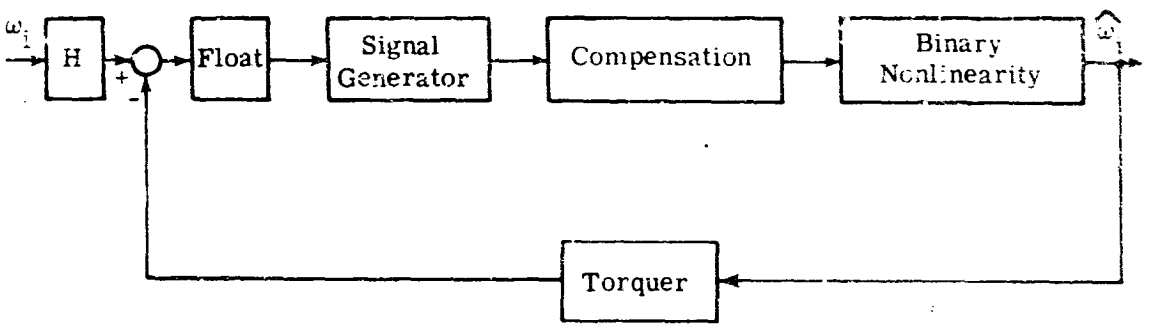

Figure 3.1-2 Position of Binary Gyro Loop Compensation

torque generator and zero order hold in the feedback path do not affect the closed loop frequency response characteristics computed.

Lead-Lag Compensation – Consider linear compensation with transfer function

$$\frac{s\alpha\tau_c + 1}{s\tau_c + 1} \qquad \alpha > 1$$

Figure 3.1-3 is an asymptotic plot of the open loop gain as a function of frequency.

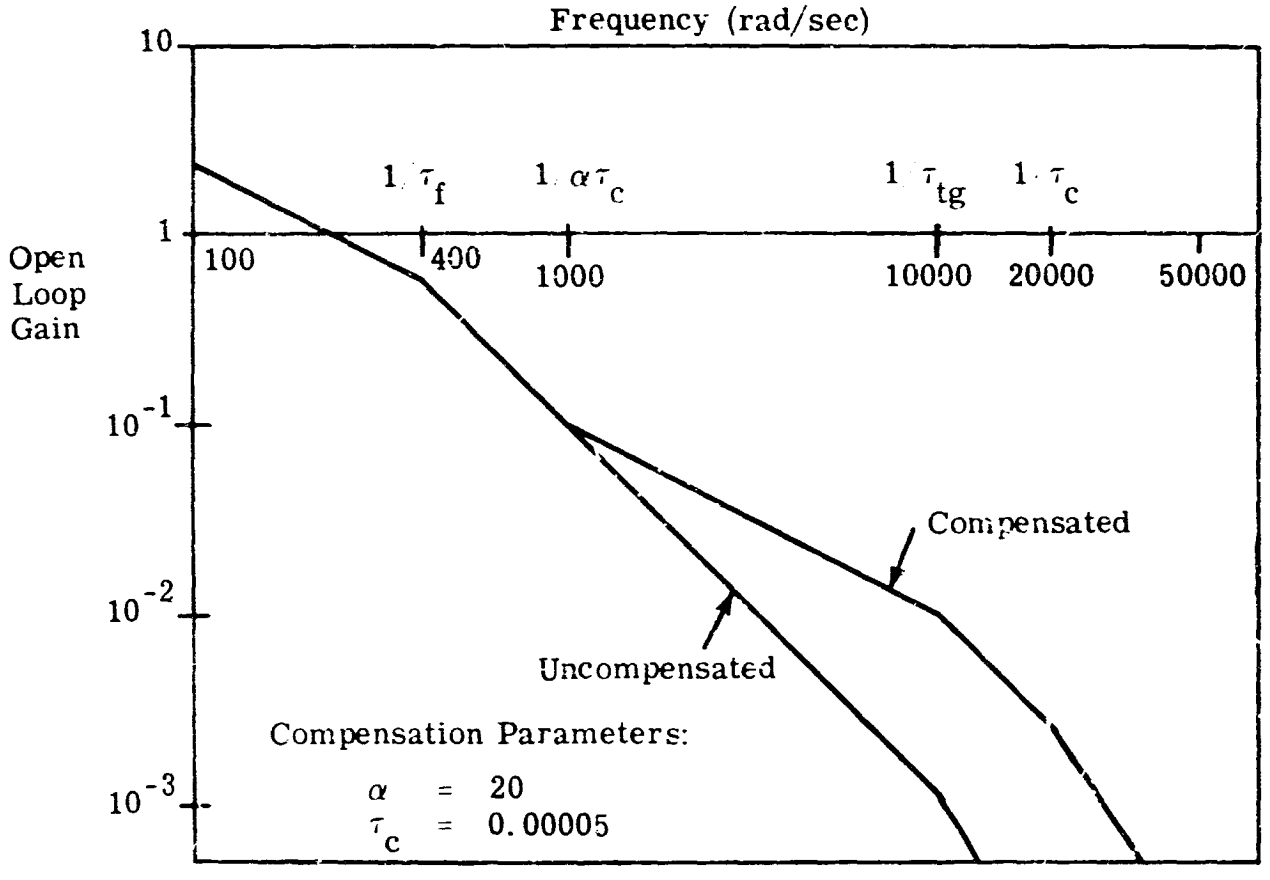

Figure 3.1-3 Open Loop Gain With Lead-Lag Compensation (Best Parameter Values)

The peak closed loop gain can be reduced, although not forced to unity, by choosing the compensation time constant to be about half that of the torquer. For this value of τ_c increasing α to a value of 20 reduces the peak closed loop gain to a minimum of about 2.5. Holding α constant at 20 and increasing τ_c to four times the float time constant raises the peak closed loop gain to a value almost as high as that of the uncompensated loop ($\cong 5$). At this value of τ_c, the effect of α variations is reversed: increasing α increases the peak gain. Lead-lag compensation does not produce a satisfactory binary gyro frequency response.

Lead-Lag-Lag-Lead Compensation – A form of compensation with the transfer function

$$\frac{(s\alpha\tau_c + 1)\left(s\frac{1}{\alpha}\tau_c + 1\right)}{(s\tau_c + 1)^2} \quad ; \quad \alpha > 1$$

was investigation. Figure 3.1-4 illustrates the gyro open loop gain-frequency characteristic with this compensation. As with lead-lag compensation, this scheme can reduce but not eliminate the closed loop peak. Large values of τ_c (between τ_f and $4\tau_f$) result in peak gains nearly as high ($\cong 5$) as in the uncompensated case. Small values of $\tau_c (\cong \tau_{tg})$ also result in poor compensation. The lowest peak gain is achieved by choosing a mid-range value for $\tau_c (\cong 0.0005 = 1/\omega_\ell$ where ω_ℓ is the uncompensated loop limit cycle frequency). With this value of τ_c, increasing α lowers the peak gain to a minimum value of about 2.2 for $\alpha = 20$. Lead-lag-lag-lead compensation offers only a slight improvement over the lead-lag compensation scheme.

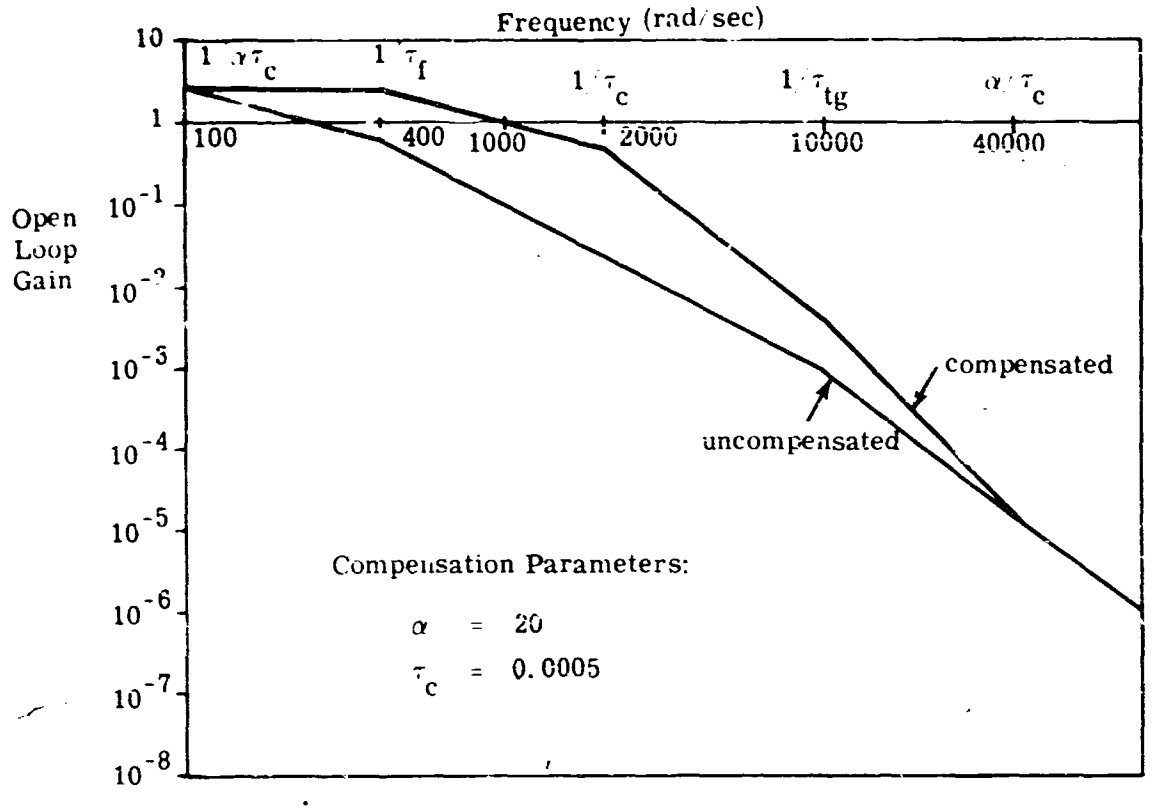

Figure 3.1-4 Open Loop Gain With Lead-Lag-Lag-Lead Compensation (Best Parameter Values)

Damped Second Order and Lag – From Fig. 3.1-1 it can be seen that the linear compensation necessary to provide an open loop gain-phase characteristic which coincides with the unity closed loop gain curve must provide rapidly increasing phase lag with little change in amplitude ratio at frequencies immediately below ω_ℓ. A resonant second order system provides rapid changes in phase shift but gives a sharp amplitude ratio peak. By cascading such a system with a first order lag to reduce the gain peak, it was

hoped that the desired gyro open loop characteristics could be achieved. Figure 3.1-5 shows the resulting open loop gain characteristic. The first two

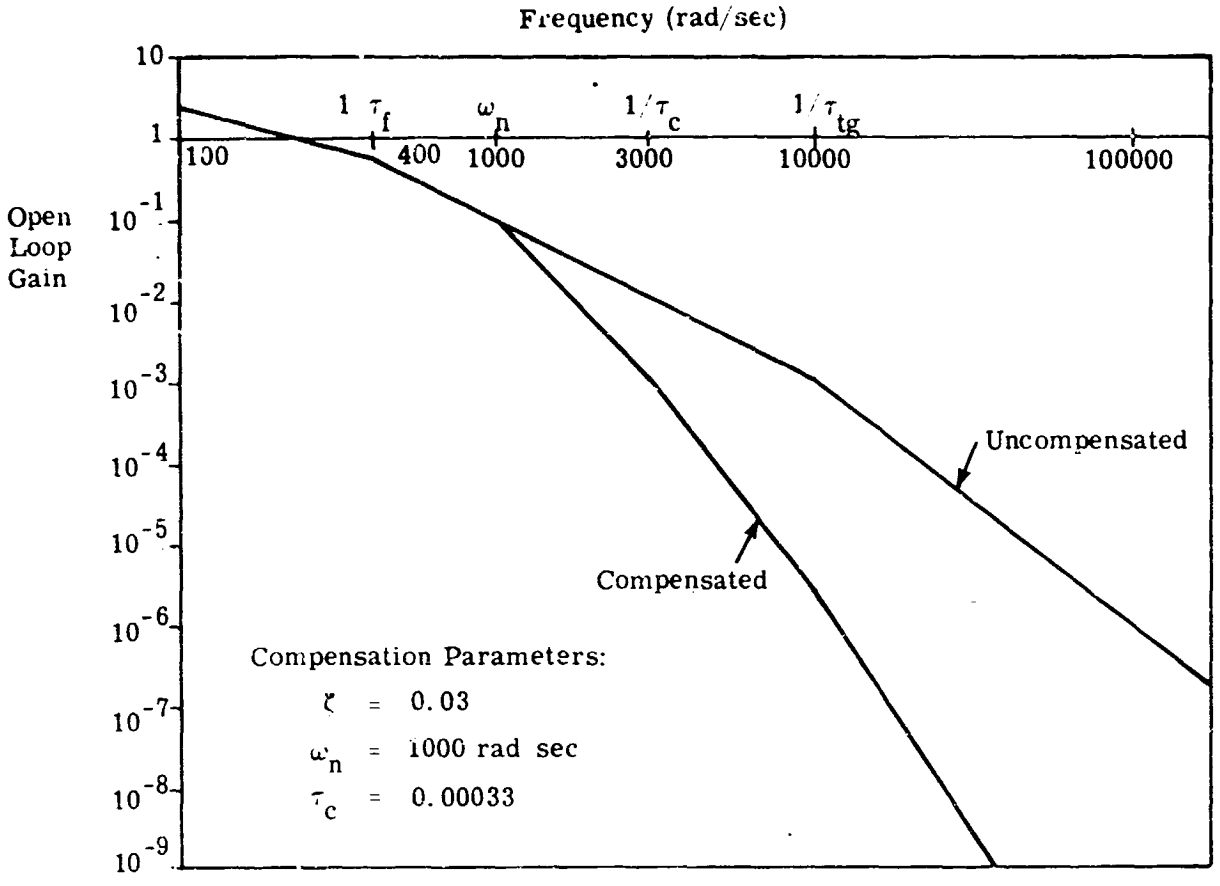

Figure 3.1-5 Open Loop Gain With Damped Second Order and Lag Compensation (Best parameter values)

compensation schemes discussed share a common characteristic; both produce closed loop amplification over the entire frequency range up to the limit cycle frequency. For the gyro parameters postulated, the damped second order plus lag compensation can also produce closed loop amplification for all frequencies

below ω_ℓ but only if one or more of the following conditions is satisfied: $\omega_n > 720$ Hz, $\tau_c > 1/\omega_n$ or $\zeta > 0.1$. Otherwise, attenuation results over some portion of the range $\omega < \omega_\ell$. This behavior is seen in Fig. 3.1-6.

Neither large amplification nor large attenuation is desirable at any frequency. In view of the fact that this compensation scheme cannot produce a perfectly flat response, the best course of action is to choose a set of compensation parameters which will minimize the maximum deviation of any part of the closed loop response from unity gain. For this example they are:

$$\zeta = 0.03$$

$$\omega_n = 159 \text{ Hz}$$

$$\tau_c = 0.00033 \text{ sec.}$$

The resulting closed loop response has a maximum gain of approximately 1.27 at 48 Hz and a minimum gain of about 0.84 at 104 Hz with a limit cycle frequency of 126 Hz. The uncompensated response has a peak of about 5 at 207 Hz and ω_ℓ = 318 Hz. The decrease in the limit cycle frequency as a result of compensation is unavoidable. Since damped second order and lag compensation only adds open loop phase lag, ω_ℓ is lowered and the usable bandwidth is always decreased when the binary limit cycling loop is compensated in this way. Because of the nature of pulsed gyro loops, the limit cycle amplitude increases when ω_ℓ becomes smaller.

Integral-Bypass Compensation – A fourth type of compensation was tried. The motivation here was not to flatten the closed loop response but to reduce the average low frequency float angle (taken over one or more limit cycle periods). Specifically, it was desired to use compensation at the nonlinearity input which approximates a pure integrator for low frequencies, thus giving the open loop a double integration characteristic for constant inputs.

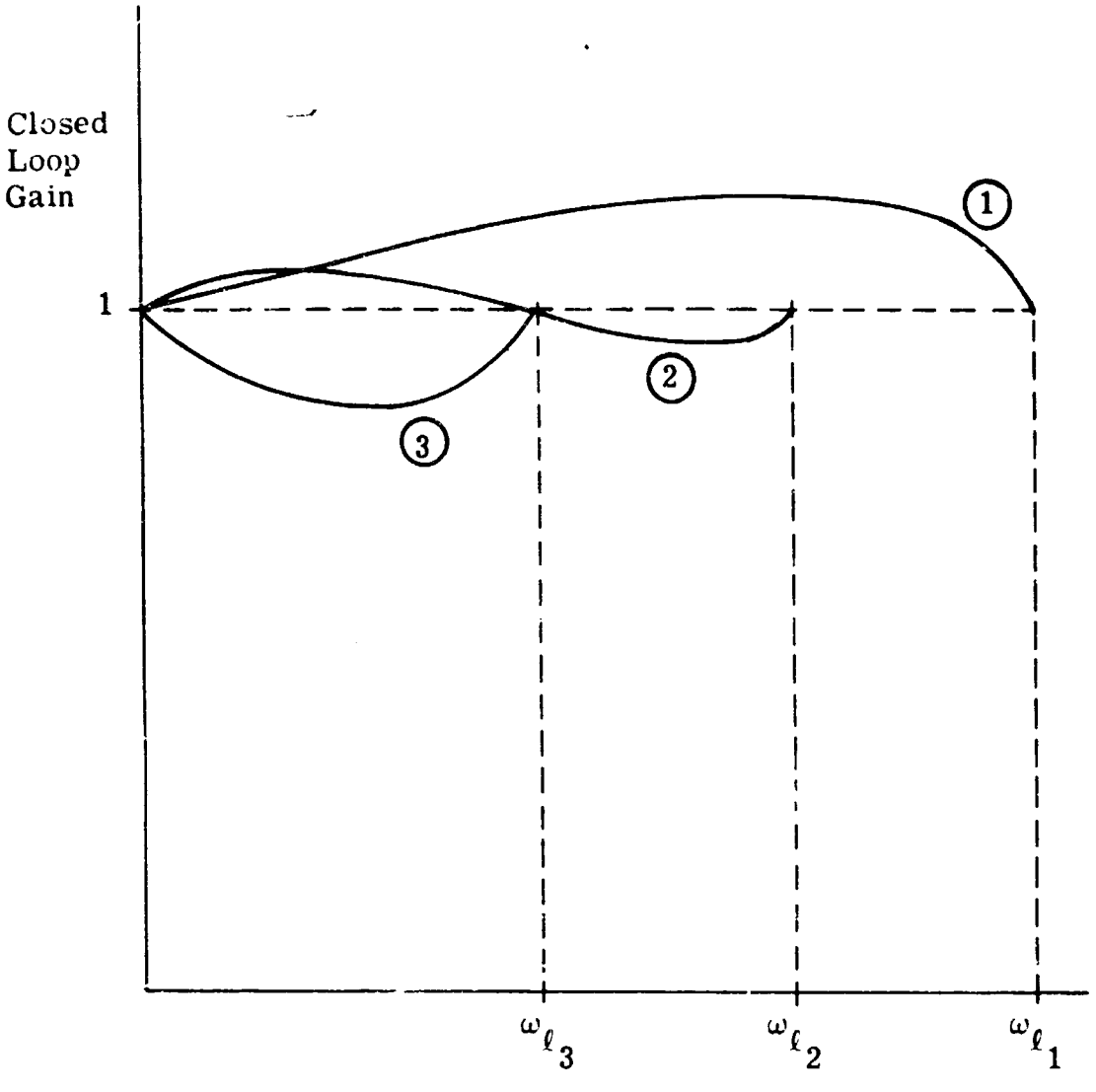

Response Number	Parameter Values
(1)	$\omega_n > 720$ Hz, $\tau_c > \frac{1}{\omega_n}$, $\zeta > .1$
(2)	$\omega_n < 720$ Hz, $\tau_c < \frac{1}{\omega_n}$, $.01 < \zeta < .1$
(3)	$\omega_n < 720$ Hz, $\tau_c << \frac{1}{\omega_n}$, $\zeta < .01$

Note: The above figure is for illustrative purposes only.

Figure 3.1-6 The Effect of Parameter Variations in Second Order Resonant Plus Lag Compensation

When the additional integration is inserted in the loop the average float angle is zero for a constant input. This compensation also reduces the float angles caused by low frequency inputs.

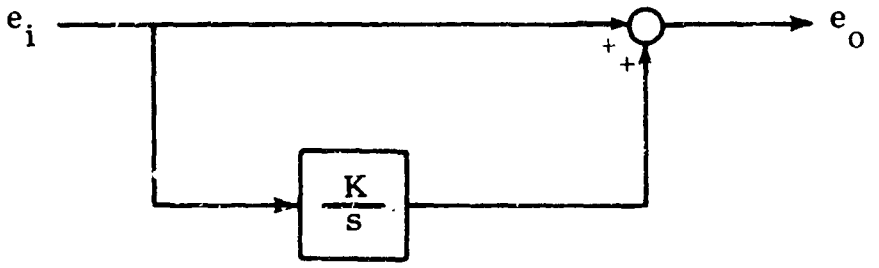

Figure 3.1-7 Block Diagram for Integral Bypass Compensation

Integral-bypass compensation (see Fig. 3.1-7) has the transfer function

$$\frac{s + K}{s}$$

The open loop gain characteristic for a gyro having this compensation is shown in Fig. 3.1-8. At low frequencies the transfer function is approximately K/s, while at high frequencies the compensation has unity gain, no phase shift and does not influence the loop response. The effect of integral bypass compensation is seen in Fig. 3.1-9 as a bending of the open loop response towards the -180° phase line at low frequencies. Increasing K broadens the frequency range over which float motion is suppressed by enlarging the frequency range over which the compensation behaves like an integrator. Note that a value of K as high as 10 has little effect on the limit cycle frequency or the closed loop

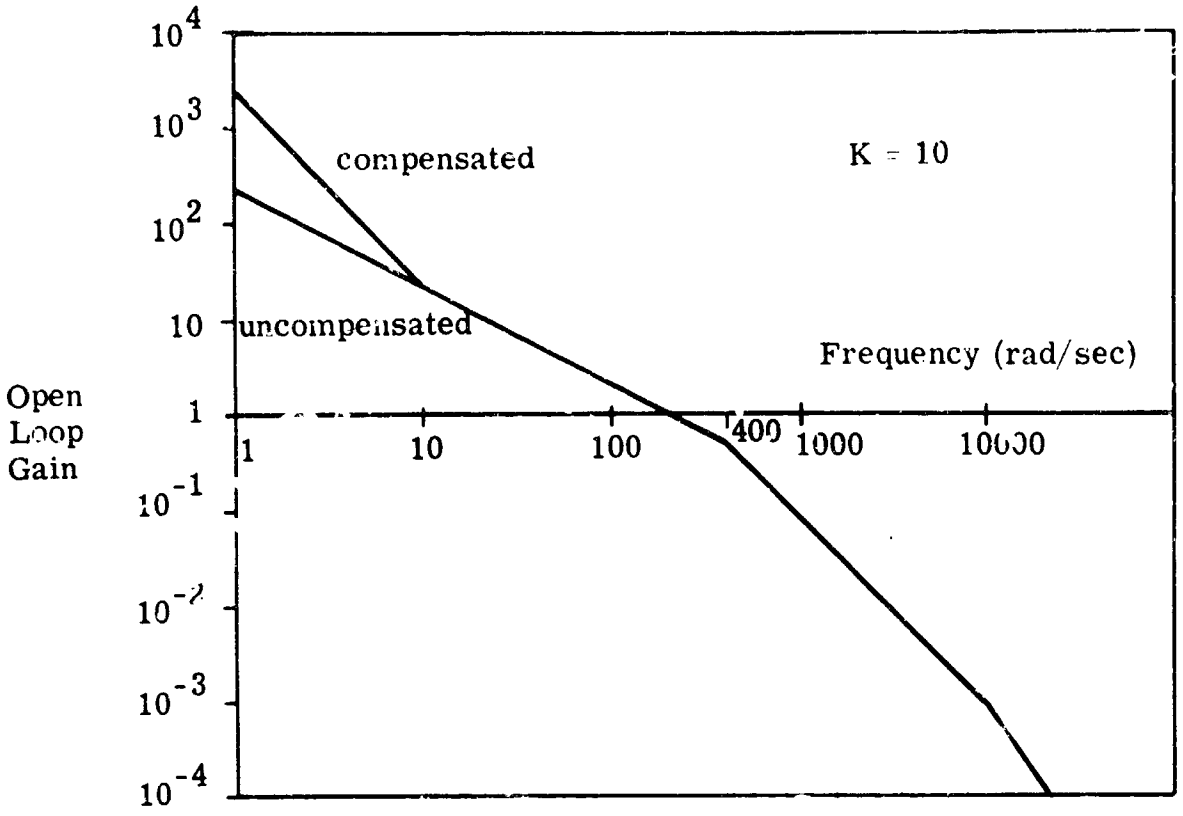

Figure 3.1-8 Open Loop Gain With Integral Bypass Compensation (Best Parameter Value)

response near ω_ℓ. Because integral bypass compensation with $K \leq 10$ has its major effect on the low frequency part of the open loop response curve where the closed loop gain is near unity, the change in overall closed loop performance is negligible. For this range of K, integral bypass compensation reduces the average float hangoff from low frequency input rates and leaves the overall closed loop response and limit cycle essentially unchanged.

Conclusion - Of the compensation schemes tried, the one composed of a damped second order and lag is most effective in reducing the peak closed

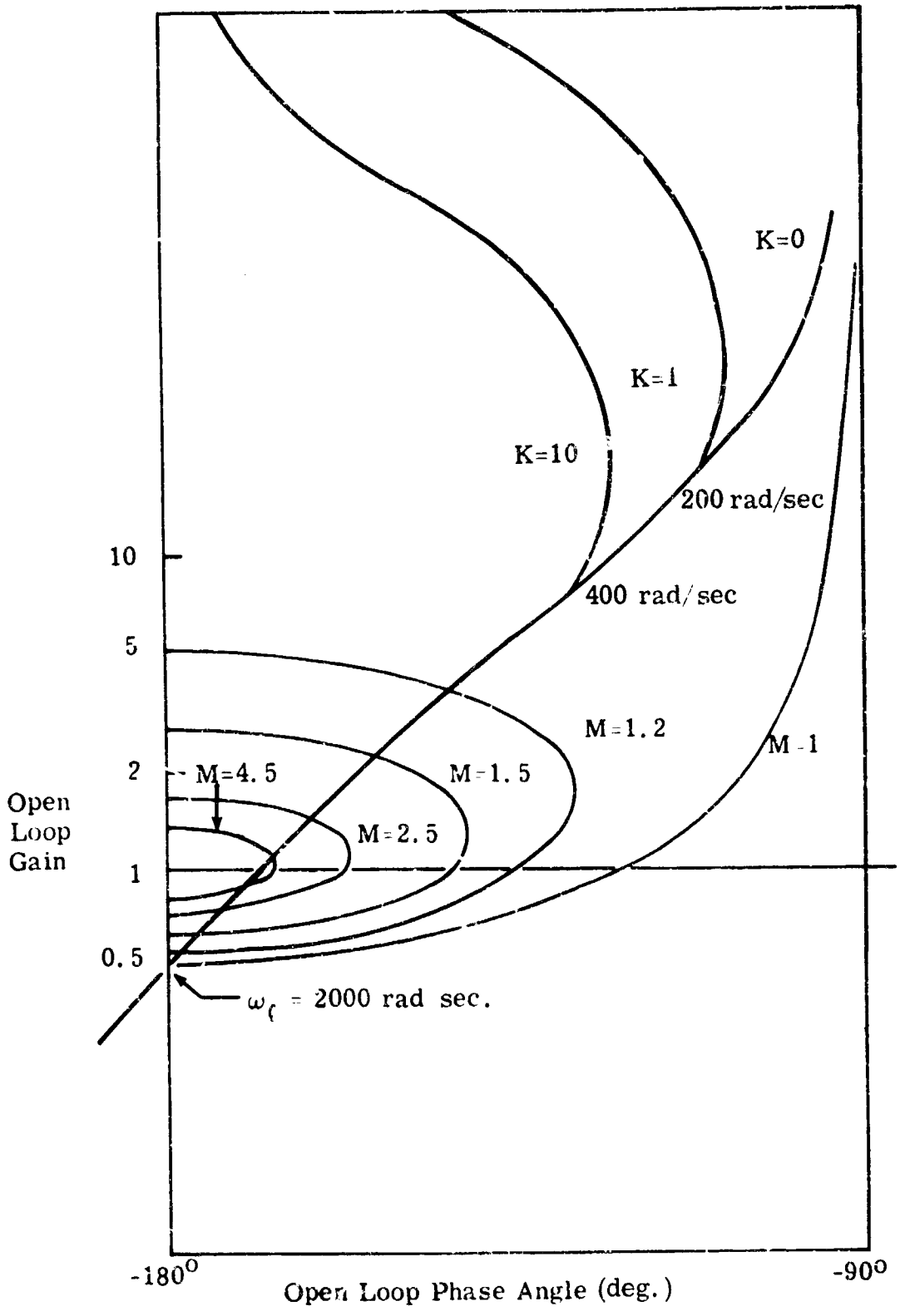

Figure 3.1-9 Nichols Chart Showing the Effect of Integral-Bypass Compensation on Open Loop Response

loop gain. Of course, the results described above are determined for a particular set of gyro parameters. Any compensation which can provide a unity closed loop response over a wide range of frequencies must contain strong lag terms in its transfer function. The most effective compensation to force the open loop gain-phase curve to lie along the M = 1 line seems to be a resonant network which causes an abrupt increase in phase lag. Because of the strong lag used in this compensation, the limit cycle frequency is lowered considerably. The result is a higher amplitude limit cycle and decreased closed loop bandwidth. Some reduction of the bandwidth may be desirable, but increasing the limit cycle amplitude is not. Larger limit cycle float motions result, and cross-coupling errors increase.

The integral bypass scheme seems efficient in eliminating low frequency float hangoff while leaving the closed loop response at the output essentially unchanged. Of particular note is the fact that the limit cycle frequency is unchanged, and the compensated gain-phase curve is identical to the uncompensated one except at low frequencies. Since integral bypass compensation modifies the signal open loop gain-phase curve primarily at low frequencies (if K < 10) and second order and simple lag compensation effects the curve at frequencies at least a decade higher, the two compensation schemes will not interfere with each other if both networks are used in cascade. In that case the closed loop gain will be near unity out to ω_ℓ and the gyro will have small gimbal angles for low frequency inputs.

The problem of forcing the gyro open loop gain-phase characteristics to approximate the M = 1 line lends itself to more sophisticated analytic techniques than were used in this investigation. Having postulated a form for the forward path compensation, any number of compensation parameters can be chosen to provide a best fit to the desired curve. For example, the area enclosed by the M = 1 line and the compensated open loop characteristic can be

minimized. However, it is not clear that the effort involved in such an approach will be justified by the improvement and practicality of the results compared with those obtained in this section.

Table 3.1-1 summarizes the compensation forms investigated and the results obtained. Figure 3.1-10 illustrates the best closed loop characteristics for different compensation networks.

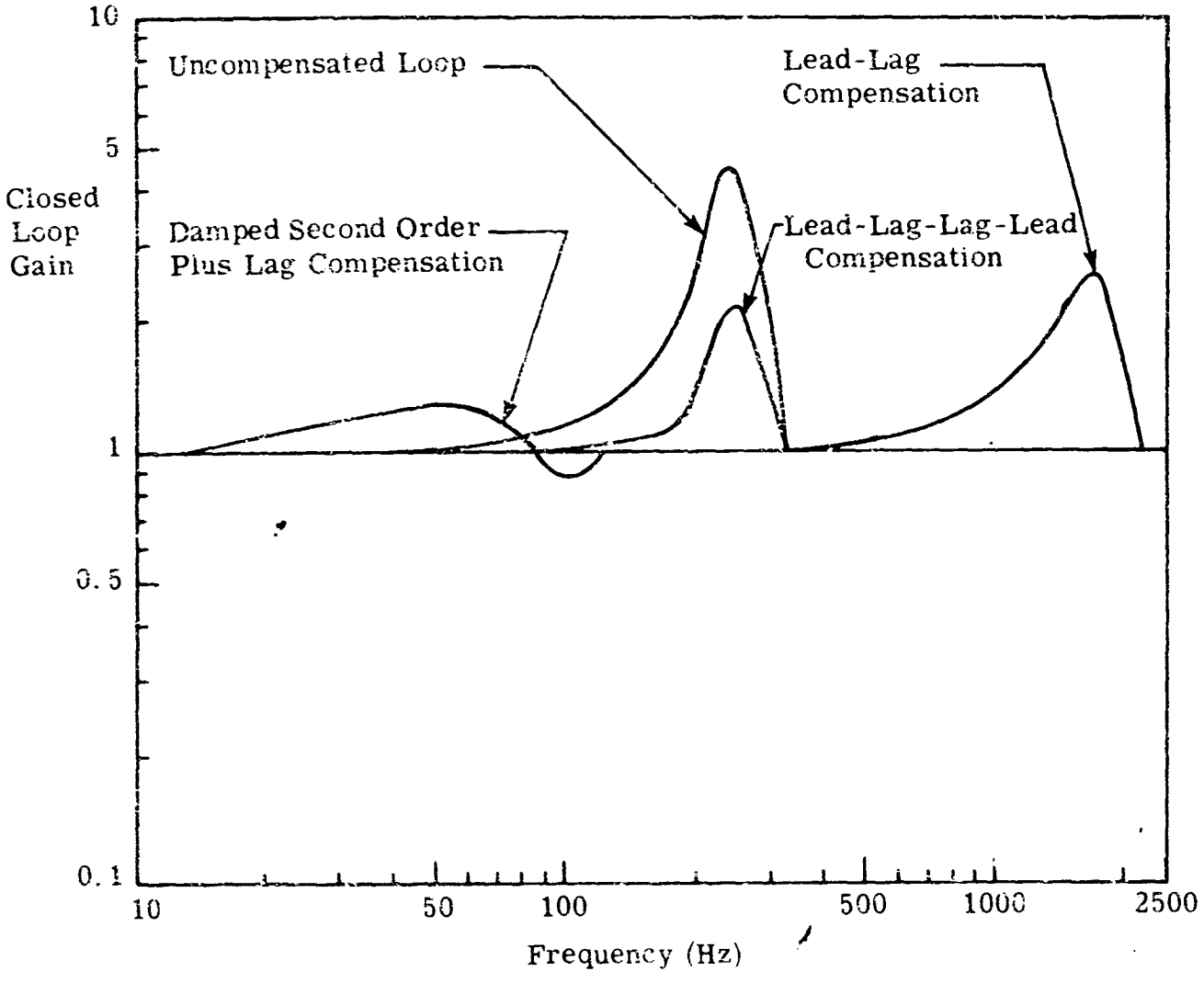

Figure 3.1-10 Best Closed Loop Gain Characteristics for Different Compensation Networks

TABLE 3.1-1

BEST BINARY LOOP RESPONSE ATTAINABLE AS A FUNCTION OF THE COMPENSATION SCHEME TRIED

Compensation	Transfer Function	Performance Criterion	Best Value Attained	Best Parameter Values
1. Lead-lag	$\frac{s\alpha\tau_c + 1}{s\tau_c + 1}$	Force closed loop gain to unity at all frequencies below that of the limit cycle	Minimum Peak Gain = 2.5	$\tau_c \cong \frac{1}{2}\tau_{tg}$ $\alpha = 20$
2. Lead-lag-lag-lead	$\frac{(s\alpha\tau_c+1)(s\frac{1}{\alpha}\tau_c+1)}{(s\tau_c+1)^2}$		Minimum Peak Gain = 2.2	$\tau_c = \frac{1}{\omega_\ell}$ $\alpha = 20$
3. Damped second order plus lag	$\left(\frac{1}{s^2+2\zeta\omega_n s+\omega_n^2}\right)\left(\frac{1}{s\tau_c+1}\right)$		(max gain = 1.27) (min. gain = 0.84)	$\zeta = 0.03$ $\omega_n = 1000$ rad sec $\tau_c = 0.00033$
4. Integral-bypass	$\frac{s+K}{s}$	Minimize float angle for low frequency inputs - leave closed loop response unchanged	No average float angle for constant inputs - stiff float for inputs to about 2 Hz. Closed loop response unchanged.	$K = 10$

$\tau_f = 2.5\times10^{-3}$ sec. $K_{sg} = 2\times10^4$ mv/rad

$\tau_{tg} = 10^{-4}$ sec. $K_{tg} = 1200$ dyne-cm/ma

$C = 10^5$ dyne-cm-sec.

3.2 LINEAR ANALYSIS OF THE DITHERED BINARY TORQUED GYRO

The addition of a dither signal to the nonlinearity input of a binary torqued gyro can be used to create an approximately linear relation between the gimbal angle, α_o, and the gyro output (see Ref. 1). Also, if attenuation of the dither oscillation by float dynamics is large enough, the dither nonlinearity can be represented as a limiter as shown in Fig. 3.2-1. Linear feedback analysis techniques can be used to investigate the transfer characteristics of the loop illustrated over a wide range of amplitudes and frequencies. However, the limiting nature of the new representation for the dithered binary nonlinearity raises the possibility of a no-imput limit cycle in the rebalance loop. Careful consideration reveals that the potential limit cycle in the dithered gyro is essentially the same unforced oscillation that occurs in any simple binary loop. Using the block diagram of Fig. 3.2-1, it can be seen that any limit cycle must have a frequency which provides π radians of phase lag in the linear part of the loop; the nonlinearity shown provides no phase change. The sinusoidal describing function for the limiter, N_A, is illustrated in Fig. 3.2-2. Peak gain occurs when the input sinusoid has an amplitude smaller than the dither magnitude, A_d. In that case the describing function is a constant, D/A_d. For a limit cycle to exist, the following relation must be satisfied:

$$N_A |H(j\omega_\ell)| = 1 \qquad (3.2\text{-}1)$$

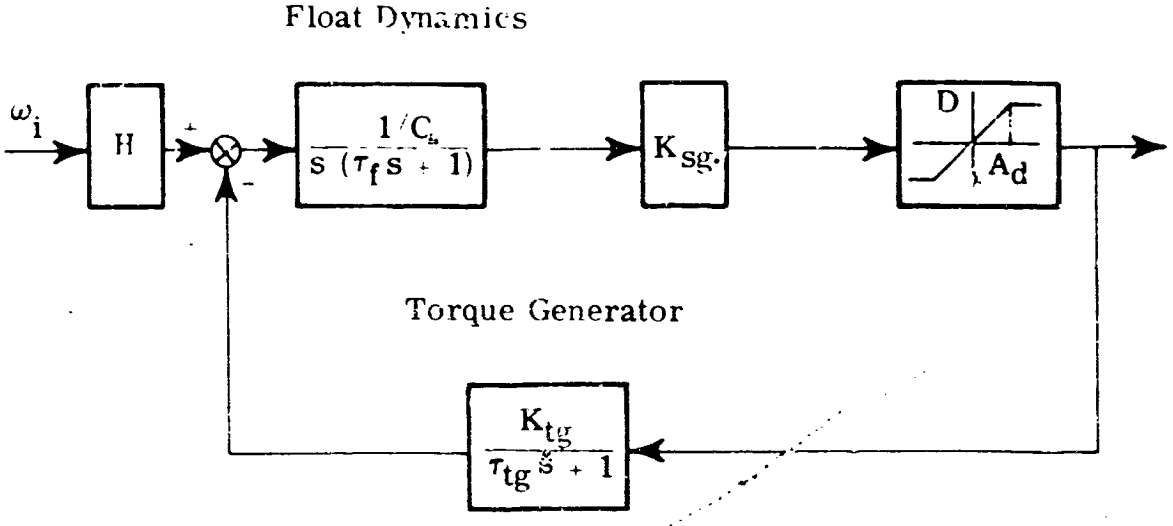

Figure 3.2-1 Dithered Binary Gyro

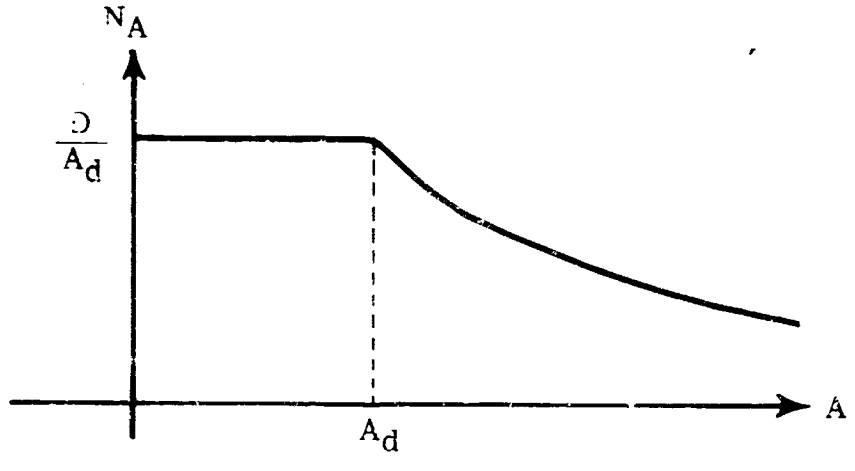

Figure 3.2-2 Describing Function for the Limiter

For the gyro model illustrated

$$|H(j\omega_\ell)| = \frac{K_{sg}K_{tg}}{C} \frac{\tau_f\tau_{tg}}{\tau_f+\tau_{tg}} \qquad (3.2\text{-}2)$$

Consequently, to prevent a limit cycle the dither amplitude must be chosen so that

$$A_d > \frac{K_{sg}K_{tg}D}{C} \frac{\tau_f\tau_{tg}}{\tau_f+\tau_{tg}} \qquad (3.2\text{-}3)$$

If the dither frequency attenuation by the float is sufficient (validating the representation of the nonlinearity shown in Fig. 3.2-1) and Eq. (3.2-3) is satisfied, the application of dither at the input to the binary nonlinearity will prevent the occurrence of a limit cycle. Analysis of the dithered gyro loop for a wide range of inputs can then proceed using techniques developed for linear feedback systems.

Example – Consider a single-degree-of-freedom gyro with the following parameters

$I_{oo} = 250$ gm-cm^2 $\qquad C = 1 \times 10^5$ dyne-cm-sec

$K_{tg} = 1,200$ dyne-cm/ma $\qquad K_{sg} = 20$ mv/m rad

$H = 2\text{x}10^5$ gm-cm^2/sec $\qquad \omega_{i_{max}} = 1$ rad/sec

Using Eq. (3.2-3), the minimum dither amplitude to preclude a limit cycle is 3.84 mv and the slope of the linear portion of the nonlinearity, $K_1 \triangleq D/A_d$, is 43.2 ma/mv. The natural frequency and damping ratio of the linearized gyro

loop are

$$\omega_n = \sqrt{\frac{K_{sg} K_{tg} K_1}{I_{oo}}} = 325 \text{ Hz}$$

$$\zeta = \frac{1}{2\tau_f \omega_n} = 0.098 \qquad (3.2\text{-}4)$$

Figure 3.2-3 illustrates the resultant frequency response for the linearized loop. For purposes of comparison the frequency response of a limit cycling binary gyro with the same parameters is shown. In interpreting the curve shown it should be remembered that for the dithered binary gyro no oscillation faster than half the dither frequency can be detected at the gyro output. This is a consequence of averaging over each dither cycle. As the dither amplitude is increased above the minimum value required to prevent a limit cycle, K_1 decreases. From Eq. (3.2-4) it can be seen that the natural frequency of the linearized gyro decreases and its damping ratio increases when A_d is made larger. The amplitude ratio frequency response for the dithered gyro is also shown in Fig. 3.2-3 for the case where dither amplitude is twenty-five times the minimum value computed above. Note the improvement over that for the uncompensated gyro.

When the dithered binary gyro is represented as illustrated in Fig. 3.2-1. the frequency response characteristics of the second order linearized rebalance loop can be controlled by varying dither amplitude. However, damping ratio and natural frequency cannot be controlled independently. Any increase in damping ratio (increase in dither amplitude) necessarily implies a decrease in natural frequency. In the example, the entire range of desirable loop transfer characteristics (ω_n and ζ) can be generated using dither signals

large enough to prevent a limit cycle. Considerably more design flexibility is available with the dithered binary gyro. In addition, the interdependence of peak closed loop gain and bandwidth can be eliminated through insertion of linear compensation in the loop. The entire range of linear systems techniques is available for analyzing the compensated loop.

The use of a dither signal with a ternary nonlinearity offers no relative advantage.

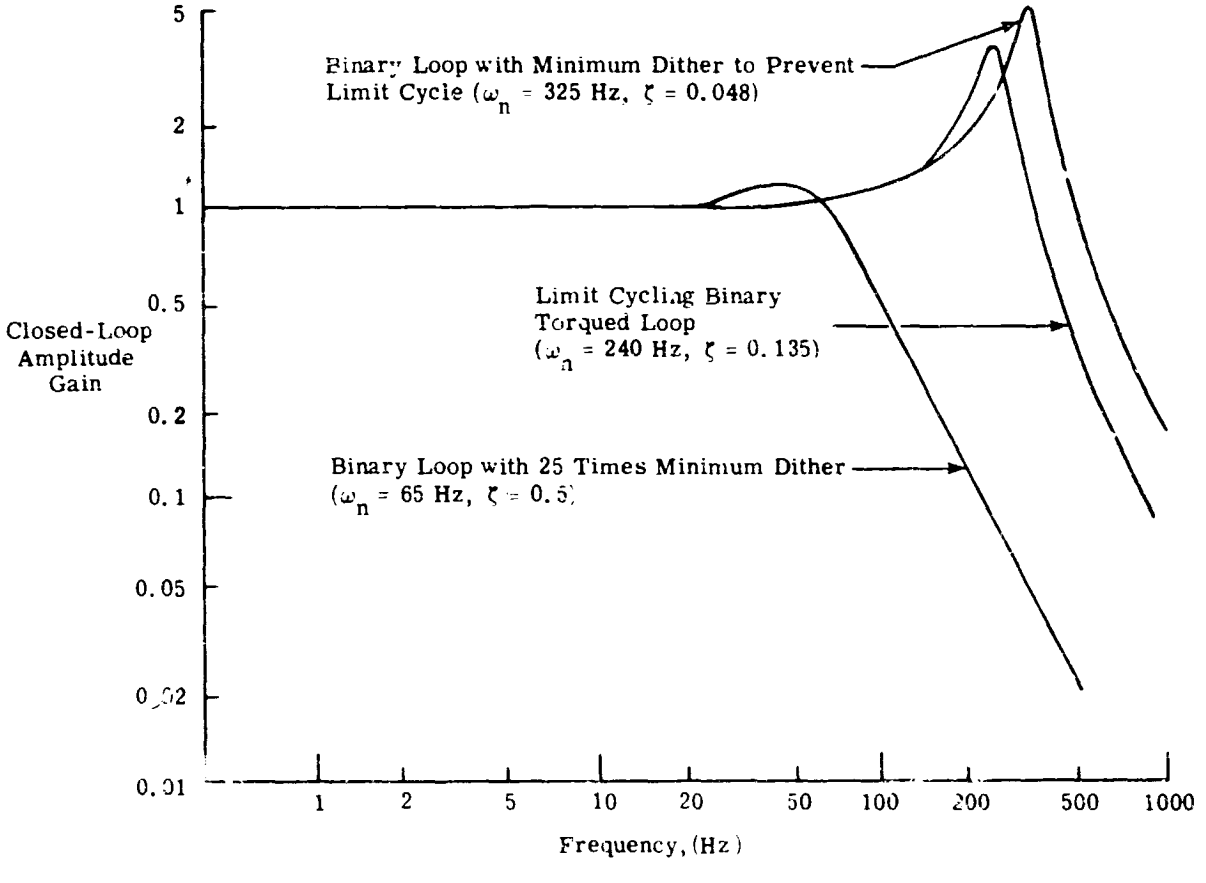

Figure 3.2-3 Frequency Response Characteristics for Binary Rebalance Loop

4. TERNARY PULSE REBALANCED GYRO LOOP

Describing function analysis was of considerable value for treating the binary gyro in Ref. 1. Similar technques are applied below to the ternary gyro of Fig. 4.1-1. Though the approach is basically the same, the effort involved is greater.

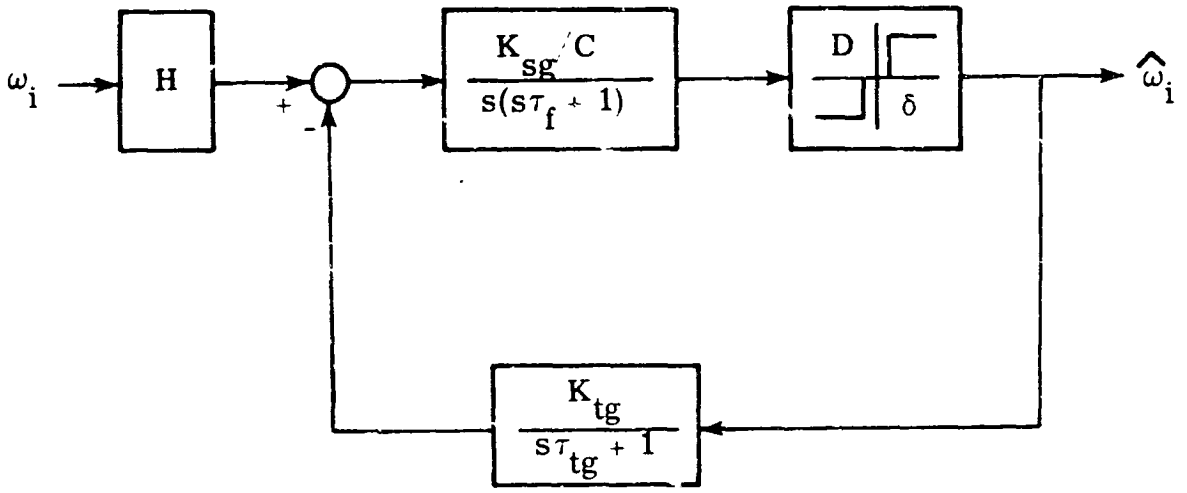

δ = dead-zone threshold in mv.

D = drive level in ma.

Figure 4.1-1 Gyro Pulse Rebalance Loop With a Ternary Nonlinearity

4.1 SINUSOIDAL FREQUENCY RESPONSE CALCULATIONS USING DESCRIBING FUNCTIONS

As in Sect. 3, we desire to make approximations which will permit application of linear analysis techniques for determining the closed loop response

to sinusoidal inputs. With the binary gyro, the presence of a limit cycle allowed us to approximate the describing function gain to a signal sinusoid by a quantity which depends only on the limit cycle amplitude (Ref. 1, 2). The closed loop frequency response to the signal was then determined by replacing the nonlinearity with the appropriate gain and applying conventional linear analysis techniques. Unfortunately, the ternary gyro does not exhibit a clearly defined limit cycle and the describing function gain of the three level nonlinearity must be treated as a function of the amplitude of the signal sinusoid entering it. Also, because the float provides frequency dependent attenuation, the amplitude of a sinusoid entering the nonlinearity is a function of both the magnitude and frequency of the gyro loop input. Consequently, a different size signal sinusoid appears at the input of the nonlinearity for each signal frequency and amplitude combination applied at the loop input. For each input combination explored in the course of a frequency response analysis, a different nonlinearity equivalent gain must be calculated and a separate determination of system output amplitude made - all to obtain one value of closed-loop gain. To simplify matters in the example, the input amplitude is held constant and only the frequency varied to obtain a plot of closed-loop gain vs frequency. However, it should be emphasized that a different plot will result from each value of input amplitude assumed.

Linearization of the Ternary Nonlinearity - The gain approximation used to describe the ternary nonlinearity is the Sinusoidal Input Describing Function (SIDF), written $N_A(A)$ and defined as the ratio between the amplitude of the fundamental sinusoid at the nonlinearity output and the amplitude A of the pure sinusoidal input to the nonlinearity. $N_A(A)$ is evaluated from:

$$N_A(A) = \frac{4D}{\pi A}\sqrt{1-\left(\frac{\delta}{A}\right)^2} \qquad (4.1\text{-}1)$$

It should be noted that the SIDF gain relates only to the first harmonic of the waveform at the nonlinearity output. All higher harmonics are ignored. They are assumed to be attenuated when passed through torquer and float dynamics. The assumption that the higher harmonics are removed by low pass elements in the loop is generally correct when treating that portion of the output signal reaching the nonlinearity input. Consequently, the closed loop analysis is not invalidated by ignoring higher harmonics at the output. However, the high frequency signals do exist at the gyro output and will enter direction cosine calculations. The frequency response curves obtained in this section account only for the first harmonic of the gyro loop output. The signal entering the nonlinearity is essentially the sum of the output fundamental and the loop input signal, both filtered by float dynamics. The sampling nature of the nonlinearity is ignored in the analysis which follows.

Describing Function Analysis: An Example - The gyro loop is divided into two parts (see Fig. 4.1-2) each of which will be treated separately to obtain certain characteristics. Then the two similar sets of relations are compared to obtain a simultaneous solution for the system. The technique is analogous to load line solutions in electrical engineering. Linear analysis is applied to the portion of the system shown in Fig. 4.1-2(a). If ω_i is a sinusoid of known magnitude, an amplitude relation can be obtained between two sinusoids of the same frequency as the input, one at point a and the other at point b. This ratio results from linear theory and does not depend on the specification of an open loop gain relation between the signals e_a and e_b (see Appendix B). When plotted for a particular gyro, the relation defines an ellipse for each different amplitude and frequency of the input sinusoid. If the input magnitude is assumed constant, a set of ellipses, illustrated in Fig. 4.1-3, results. Each ellipse represents a different input frequency.

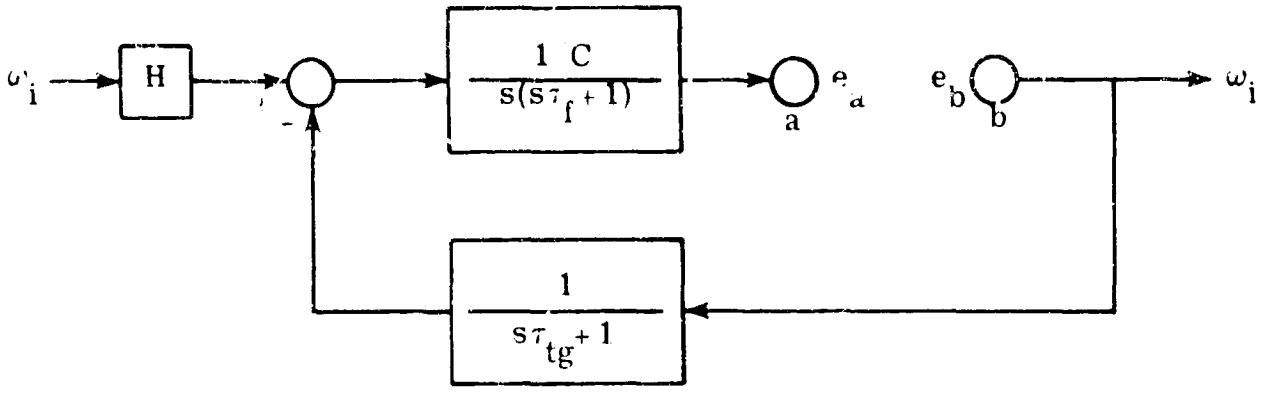

(a) Linear Part of the Loop

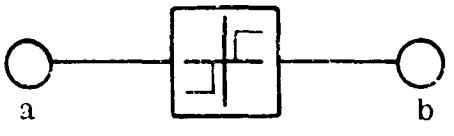

(b) Nonlinear Element

Figure 4.1-2 Pulse Rebalance Loop Divided into Linear and Nonlinear Parts

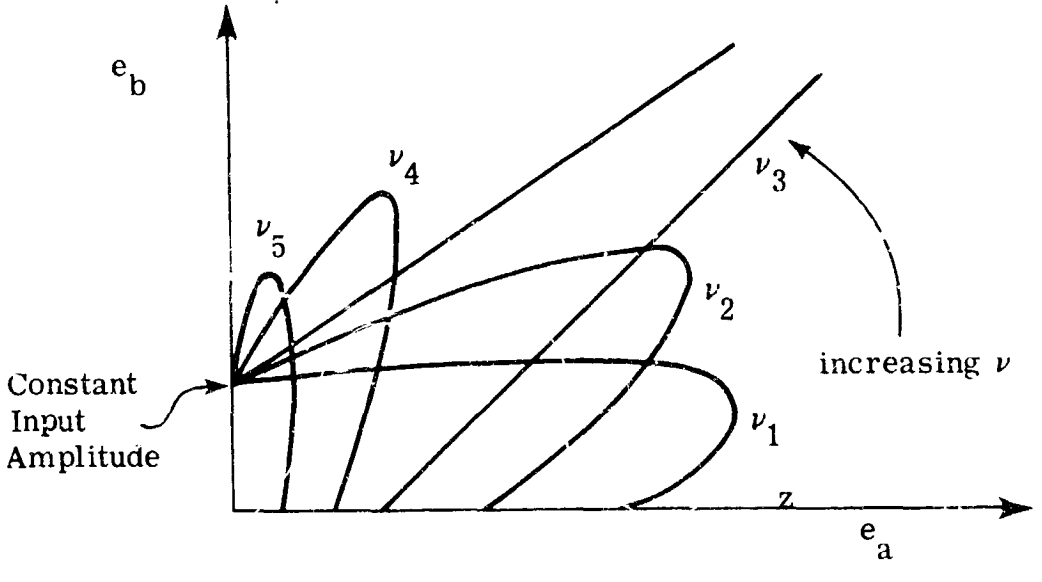

Figure 4.1-3 Ellipses Resulting From Analysis of the Linear Portion of the Loop

The ternary nonlinear element is treated separately (see Fig. 4.1-2 (b)). The describing function, Eq. (4.1-1), is used to obtain a relation similar to that computed from linear system theory. This characteristic, illustrated in Fig. 4.1-4, depends on the quantities D and δ. When the plots of Figs. 4.1-3 and 4.1-4 are superimposed, the points at which the two figures intersect constitute a set of operating points for the system. However, not all of the intersections represent stable solutions. The superposition of the two figures is shown in Fig. 4.1-5. Since each ellipse represents a different loop input frequency, each intersection point on an ellipse represents a loop operating point at that frequency. Every intersection point also supplies a particular value for the nonlinearity output. Since the output of the nonlinearity is also the loop output, the absolute value of the loop transfer function is simply e_b divided by the input amplitude. The ratios obtained for the ellipse of a particular frequency, ν, represent possible closed loop system gains to a sinusoid at that frequency.

By determining a sufficient number of intersection points it is possible to construct a closed loop amplitude ratio response curve for the ternary gyro. Figure 4.1-6 illustrates such a curve drawn from the intersection points determined in Fig. 4.1-5. The peaked portion of the closed loop response curve exhibits a "jump resonance" characteristic similar to that given by a softening spring. The effect of the dead zone on the closed loop gain is seen as an abrupt drop to zero at the frequency ν_c. If there was no dead zone, the response gain would fall off gradually with increasing frequency. However, the dead zone causes the relay to block all signals below δ in amplitude at the nonlinearity input. As frequency increases, the float attenuation increases until, at frequency ν_c, signal amplitude is less than δ at the nonlinearity input. Then the output, and consequently the loop gain, drops abruptly to zero. Dead zone also causes the overhanging nature of the response curve. At high input frequencies, attenuation by float dynamics prevents the

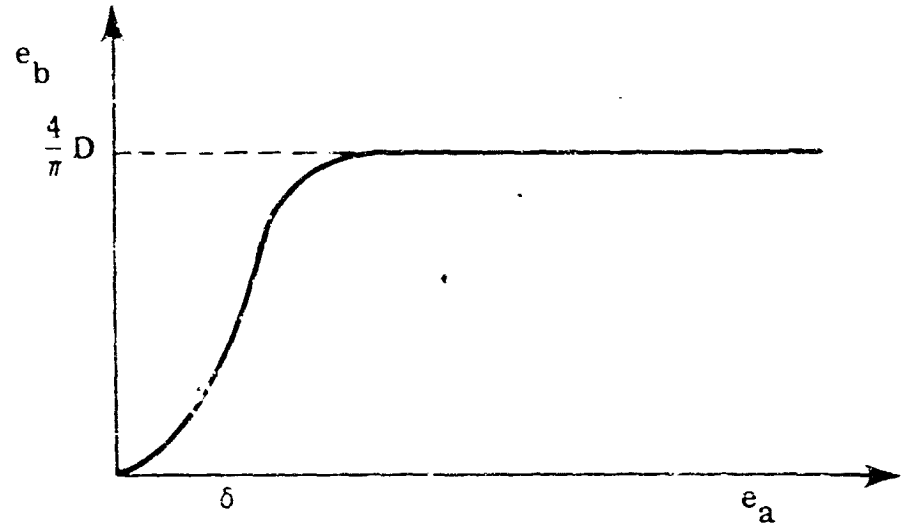

Figure 4.1-4 Output vs Input Computed from the SIDF Gain for the Nonlinearity

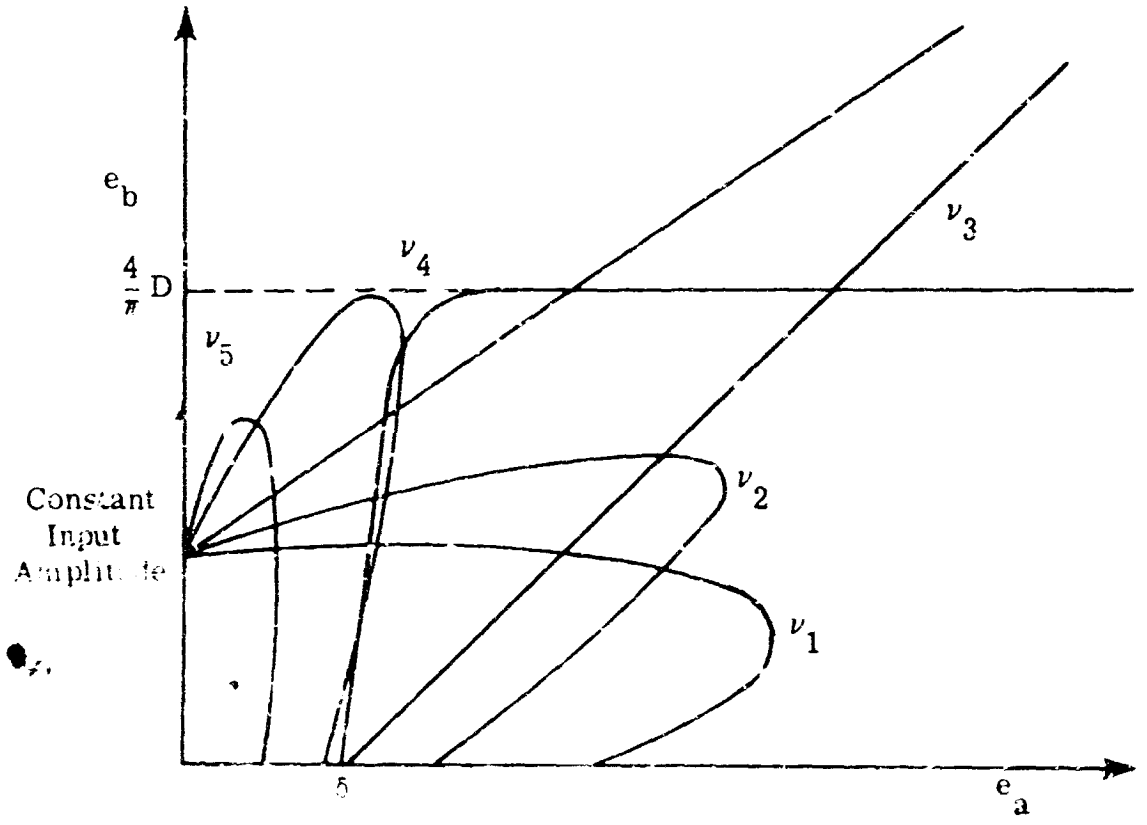

Figure 4.1-5 Superposition of Figs. 4.1-3 and 4.1-4 Showing Intersection Points.

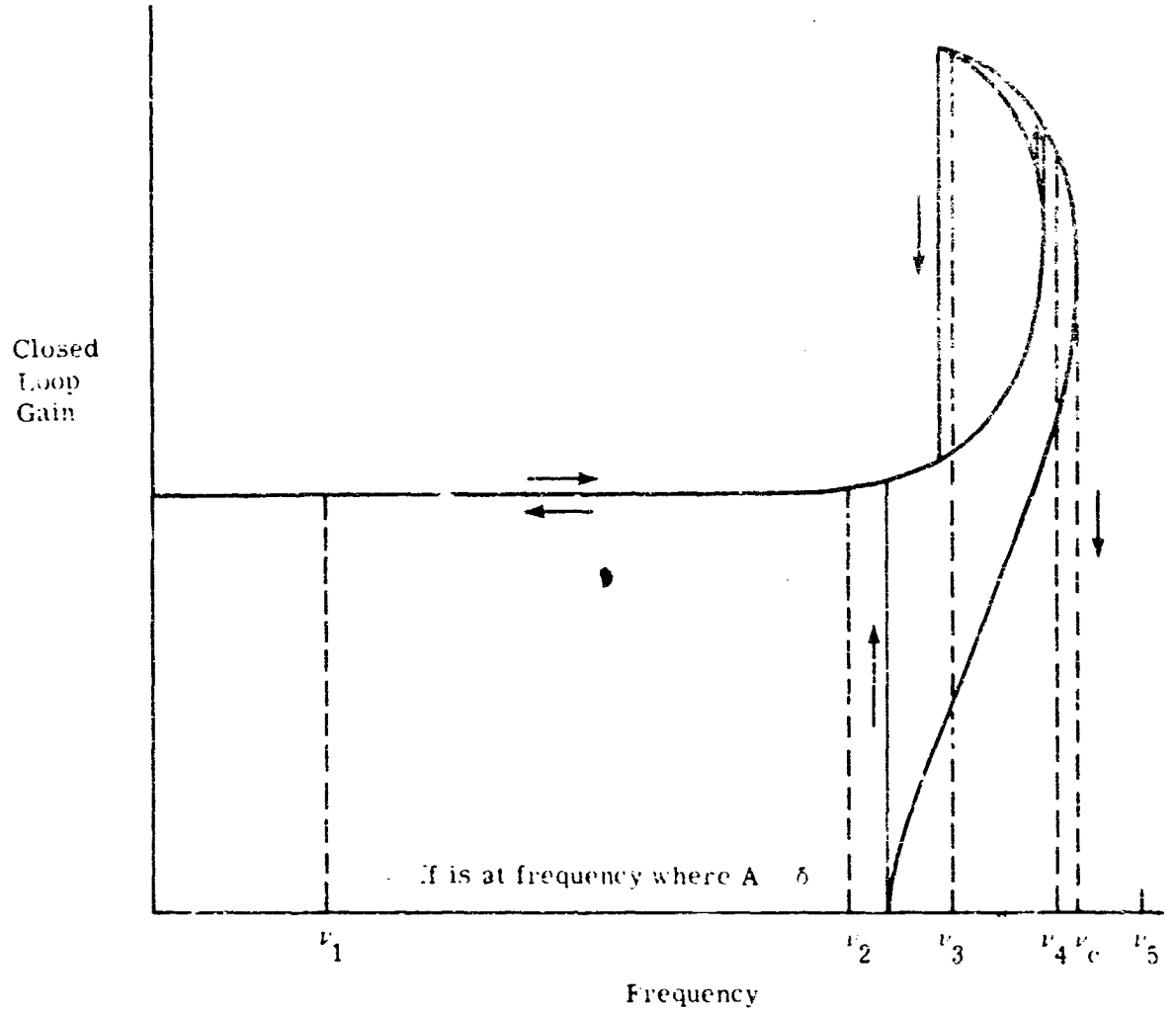

Figure 4.1-6 Ternary Gyro Closed Loop Gain

input to the nonlinearity from exceeding δ. As frequency is decreased the float angle eventually becomes larger than the dead zone, providing a loop output and generating signals at all points in the loop. This point occurs at a frequency lower than ν_c because the gyro is essentially an open loop system until an output appears at the nonlinearity.

Effect of Input Amplitude - Because the nonlinearity it contains has an amplitude dependent output, the ternary gyro loop exhibits amplitude dependent characteristics. When plotted for different magnitudes of the input sinusoid, the frequency response curves have various shapes (see Fig. 4.1-7). If the input amplitude is small enough (0.01 rad/sec in the figure) the closed loop response has no peak. As the size of the input increases the jump resorance characteristics and dual gain cutoffs discussed above become more pronounced. A look at Fig. 4.1-5 provides an explanation. The ellipsoidal curves obtained from linear analysis are changing size and rotating. As frequency increases, the length of the major axis first increases, then declines. However, rotation of the major axis is monctonic For the smallest input amplitude plotted in Fig. 4.1-7 no appreciable rotation of the constant frequency ellipses takes place before the loop output drops to zero. When the gyro output is raised to 0.03 rad/sec the ellipses rotate and the intersection points occur at higher values of e_b, giving a peaked loop response When the largest input is analyzed, the ellipses not only rotate but also become long enough to provide several intersection points at some frequencies. A jump resonance characteristic results. The describing function analysis outlined above provides a useful tool for analyzing ternary gyro loops.

4.2 EFFECT OF A RANDOM SIGNAL AT THE NONLINEARITY INPUT ON THE FREQUENCY RESPONSE

In this analysis we demonstrate how to obtain the closed loop sinusoidal response of the ternary gyro when a Gaussian random signal is present at the nonlinearity input along with the sinusoid. The random signal, described by its standard deviation, σ_r, can be present as a result of a random input to the gyro, noise in the loop or deliberate injection in the form of a random dither. The present discussion makes no assumption about the origin of the random signal.

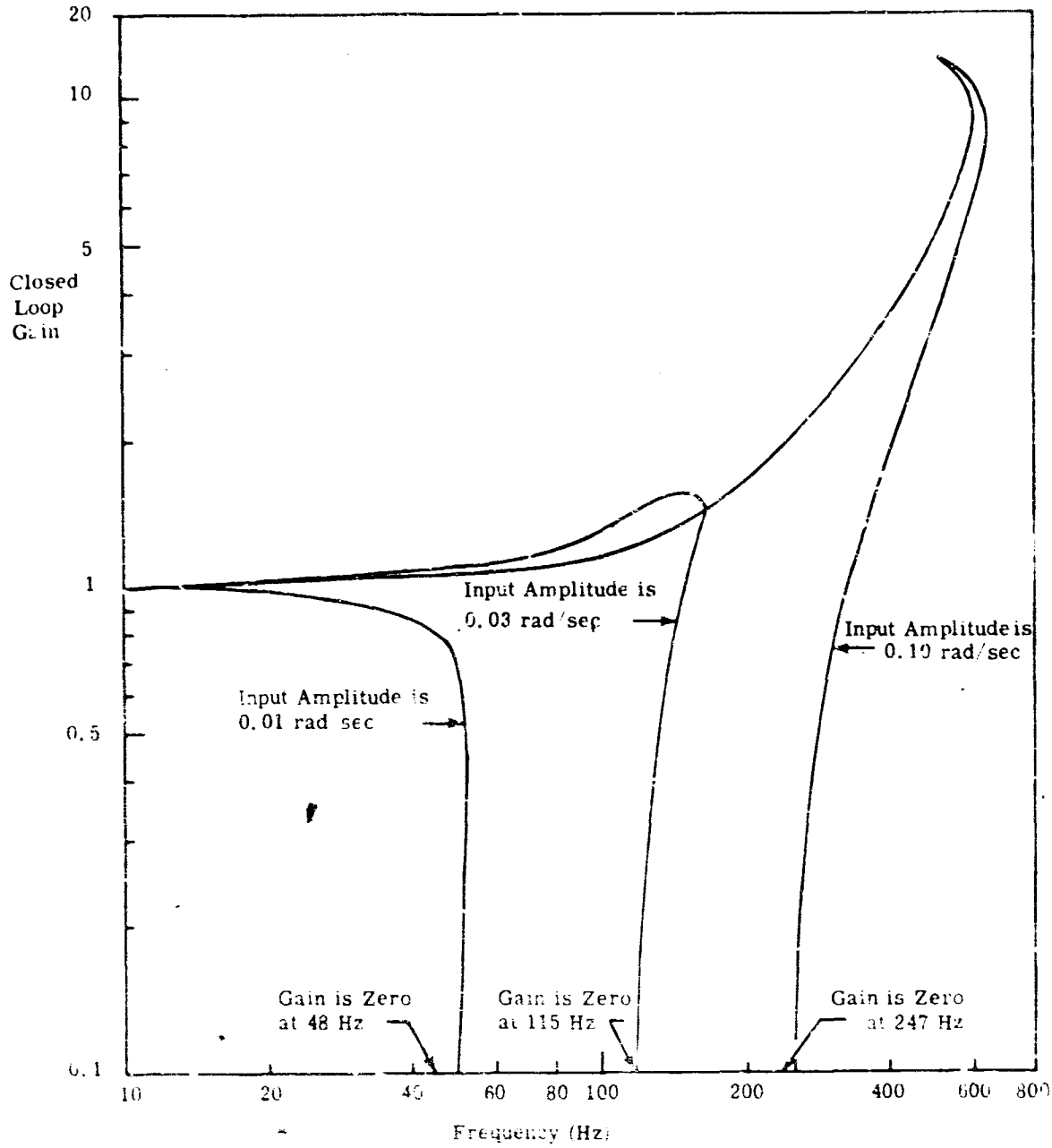

Figure 4.1-7 Effect of Input Amplitude on Closed Loop Gain

The Describing Function - Due to the presence of a random signal in addition to the sinusoid, the describing function gain to the sinusoid is different from that used in the previous section. It depends not only on the amplitude A of the sinusoidal input to the nonlinearity but also on the magnitude of the random input. A random signal can be described by its statistical moments. If it is assumed to be a Gaussian, zero mean variable its distribution is completely specified by a standard deviation, σ_r, and the describing function for the sinusoid is written as $N_A(A, \sigma_r)$. This function is given for the ternary nonlinearity in Appendix E of Ref. 3. As σ_r approaches zero $N_A(A, \sigma_r)$ becomes the describing function for a pure sinusoidal input. Figure 4.2-1 illustrates the effect of the random input on the sinusoid transfer characteristics of the ternary nonlinearity. It is similar to Fig. 4.1-4. The output characteristic shown is the average amplitude of the output harmonic of the same frequency as the sinusoidal input. The effect of a random input to the ternary nonlinearity is to make the rise of the sinusoidal input-output curve more gradual. When $\sigma_r > 0$ and $A < \delta$ there is a finite probability that the net input to the nonlinearity will exceed δ and have the same sign as the sinusoid. There is a smaller probability that it will exceed the dead zone with the opposite sign. When the mean is taken, a non-zero average value for the appropriate nonlinearity output harmonic results. In this way the sinusoid is boosted through the dead zone by the random signal. On the other hand, when A exceeds δ the fact that the net input to the nonlinearity can have a sign opposite to that of the sinusoid produces a describing function gain somewhat lower than that occuring in the absence of random signals. It can be seen from Fig. 4.2-1 that the net effect of adding a random signal at the nonlinearity input is to make the describing function gain for the sinusoid less am[illegible]

Unfortunately, the presence [illegible] more than just a change in N_A. Strictly speaking, [illegible] predicted

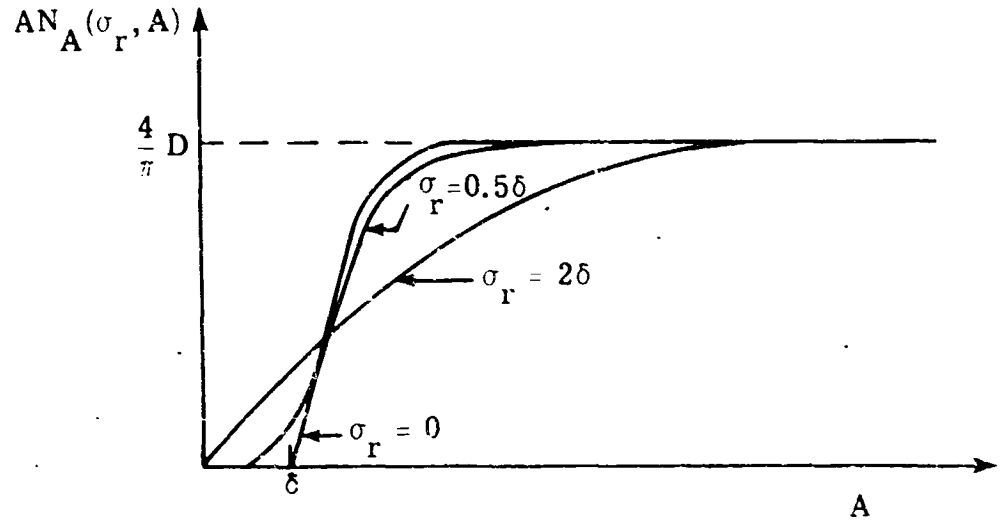

Figure 4.2-1 Effect of a Random Input on the Sinusoid Transmission Characteristics of a Ternary Nonlinearity

through the use of a describing function gain $N_r(A, \sigma_r)$ and knowledge of the characteristics of the random signal at the point where it enters the gyro loop. Since N_A and N_r both depend on A and σ_r, solution of the closed loop relations in the presence of both a sinusoid and a random signal requires a complicated iterative procedure. However, in order to illustrate the effect of random inputs to the nonlinearity we will assume different values of σ_r without specifying their origin.

The fact that the [illegible] represent the average response to a given sinusoid does not affect their value. If we are interested in the effect of gyro output on a resident model [illegible] direction cosine matrix calculation or on the system drift rate generated, [illegible] value representation is often as useful as an exact one.

Changes in the Frequency Response - Figure 4.2-2 indicates the ellipse intersection points for the sinusoid input-output curve which results when a random signal also enters the nonlinearity. Note that the likelihood of multiple intersection points occuring on any one ellipse is reduced. In this particular example there are no multiple intersection points. Also, because there can be an output for $A < \delta$, all ellipses have at least one intersection point. The effect on the sinusoid frequency response is illustrated in Fig. 4.2-3. Since no ellipse has mutltiple intersections, there is only one value of closed loop gain at each frequency; the jump resonance phenomenon is eliminated. Also the closed loop gain is greater than zero for all

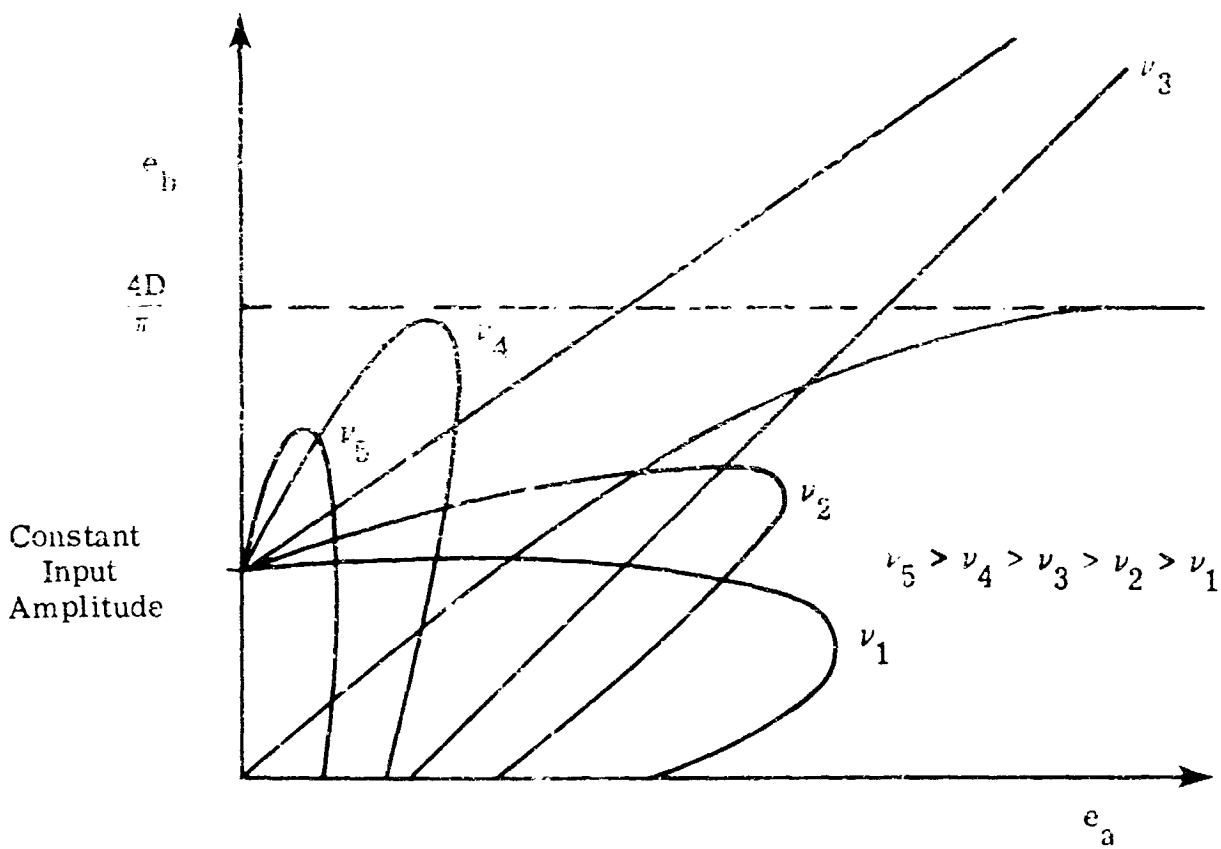

Figure 4.2-2 Ellipse Intersection Points Caused by Random Nonlinearity Input

frequencies and the sharp cutoff found in Fig. 4.1-4 is eliminated. Figure 4.2-4 shows the three frequency responses corresponding to the three nonlinearity curves of Fig. 4.2-1. As σ_r increases, the jump resonance disappears, and bandwidth increases. Gradual gain reduction at high frequencies replaces the sharp attenuation. In short, when the random signal is present, the closed loop frequency response appears to be more like that of a linear system.

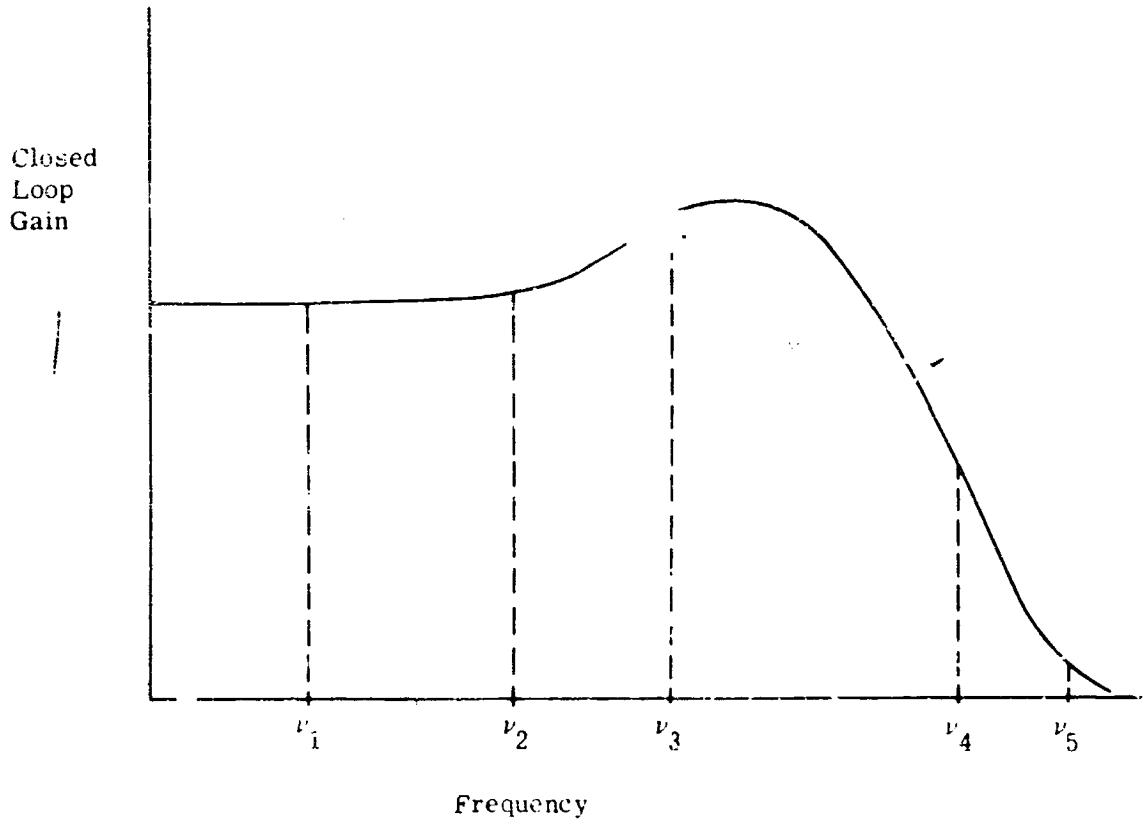

Figure 4.2-3 Closed Loop Response for a Ternary Gyro With Random Nonlinearity Input

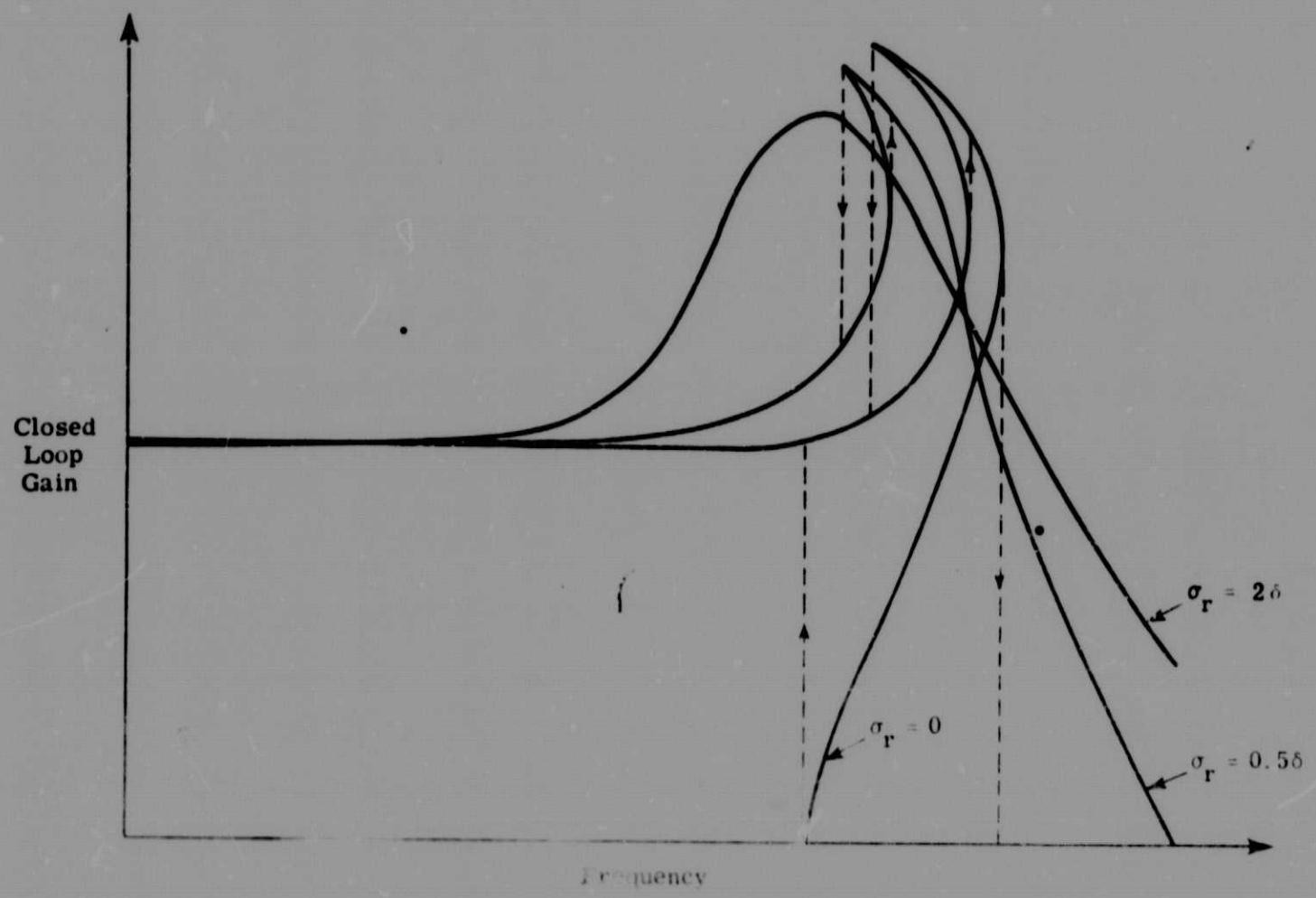

1.2-4 The Effect of σ_r on the Closed Loop Gain

5. GYRO AND SYSTEM ERROR SIMULATION

5.1 MOTIVATION FOR A SIMULATION

The analysis and results reported in Refs. 1 and 2 are based on several assumptions and simplifications. Before proceeding with further work based on those results it would be prudent to establish some check on the validity of prior approximations. While simulation is not a perfect substitute for the construction and testing of hardware it is considerably less expensive and far more versatile. As an intermediate step between analysis and prototype construction, simulation is ideally suited to the present stage of the investigation.

Topics which were treated in an approximate manner during the prior analysis include crosscoupling errors, gyro structural dynamics, random vehicle angular motions and closed loop characteristics of pulse torqued gyros. When crosscoupling errors were computed in the case of oscillatory angular motion, the gimbal output angle was obtained from a linearized model for the binary pulse torqued gyro. The linear sensor approximation does not take into account the pulsed nature of the rebalance torque or float angles generated by limit cycling. In addition, treatment of crosscoupling errors in the ternary pulse torqued gyro is very difficult even with the aid of describing function techniques. The nonlinear nature of pulse rebalanced gyros does not permit confidence in the results obtained from analysis of crosscoupling effects unless they are substantiated by simulation.

The simple model of wheel and gimbal dynamics used in almost all the previous investigations ignores the lightly damped structural vibrations which can occur. Though these vibrations lend themselves to mathematical

description as linear dynamic effects, their inclusion makes the analysis of the gyro loop behavior considerably more complex. Even the simple determination of their effect on limit cycles in a binary gyro led to the curious indication that three limit cycles with the same amplitude but different frequencies were mathematically possible. Whether the two additional limit cycle modes will in fact occur is an appropriate subject for a simulation study. Indeed, through simulation, it should be possible to determine when and if structural dynamics are of any major importance in strapdown gyros.

In the portion of Ref. 1 dealing with the gyro parameter optimization, several approximations and simplifications were made to permit easy calculation of gyro errors caused by random vehicle angular motions. A simulation which generates realistic analogs of random angular motion about all major sensor axes is needed to check the assumptions. In addition, nonlinear simulation of the sampled switching logic found in pulse rebalanced gyros will be useful in evaluating sensor closed loop transfer characteristics and to check the validity of the continuous signal describing function analysis used in the past.

Several questions which arose and were left generally unanswered in the preceeding work can be treated easily by a well designed simulation. In the discussion of strapdown gyro error compensation, the possibility of using the three basic gyros to measure angular motion for their own compensation is treated. Stability and accuracy analyses of this approach are very difficult to perform analytically because many closed loops, often containing time-varying gains, are generated. However, the technique is so attractive in terms of cost, power, weight and reliability that it must not be ignored for this reason. A well designed simulation of three gyros and the compensation calculation will permit an empirical determination of the feasibility of this approach. In addition, simulation provides an inexpensive way of checking all proposed gyro error

compensation schemes, including their sensitivity to the accuracy of various motion sensors.

In the work reported by Refs. 1 and 2, a system level figure-of-merit was developed to indicate the effect of gyro errors on strapdown system accuracy. Equations were developed relating the time histories of gyro errors to system attitude error. These expressions were exercised in the case of certain easily described gyro output errors (bias, white noise, oscillations, etc.) to give simple analytic relations between sensor and system drift rates. When examples were presented and parameter optimization was illustrated the latter relations were used rather than the original more complex equations which require complete specification of gyro error and system attitudes histories. The approximation which results is a fit subject for validation by simulation.

In addition to verifying results from prior analyses, a well designed flexible simulation will be invaluable in the continuing study of strapdown sensors. Compensation within the gyro loop is easily analyzed and the effects of various torque generator characteristics on system errors can be studied. Test procedures for determining basic sensor error parameters can be evaluated. Using the simulation, dynamic test inputs can be designed and simulated information will be available for use in comparing different test data reduction techniques. Finally, the versatility and flexibility of a simulation must be emphasized. While the ultimate verification still lies in construction and testing of actual hardware, when it is still desirable to investigate many proposed changes in gyro parameters only, simulation provides an inexpensive and expedient means.

Description of the Projected Simulation -- The simulation planned and under construction is illustrated in Figure 5.1-1. Investigation indicates that a purely digital simulation will be too slow when numerical integration is

used with the complex, high frequency dynamics to be simulated. On the other hand, the system error is to be computed using the error growth difference equations described in Ref. 2. This requires a digital computer. The hybrid simulation shown permits simultaneous determination of high frequency variables and accurate calculation of system error growth. Three gyros, including pulse rebalance torquing, will be simulated on the analog portion along with random and deterministic motion in three dimensions, gyro motion-induced error torques and error compensation schemes. The gyro models will include structural dynamics when desired. Sensor outputs and true angular motion will be provided to the digital portion for calculation of system attitude errors. The simulation described remains a flexible tool for analyzing additional aspects of strapdown sensor errors. The gyro models can be changed to accommodate studies of exotic sensors as well as accelerometers.

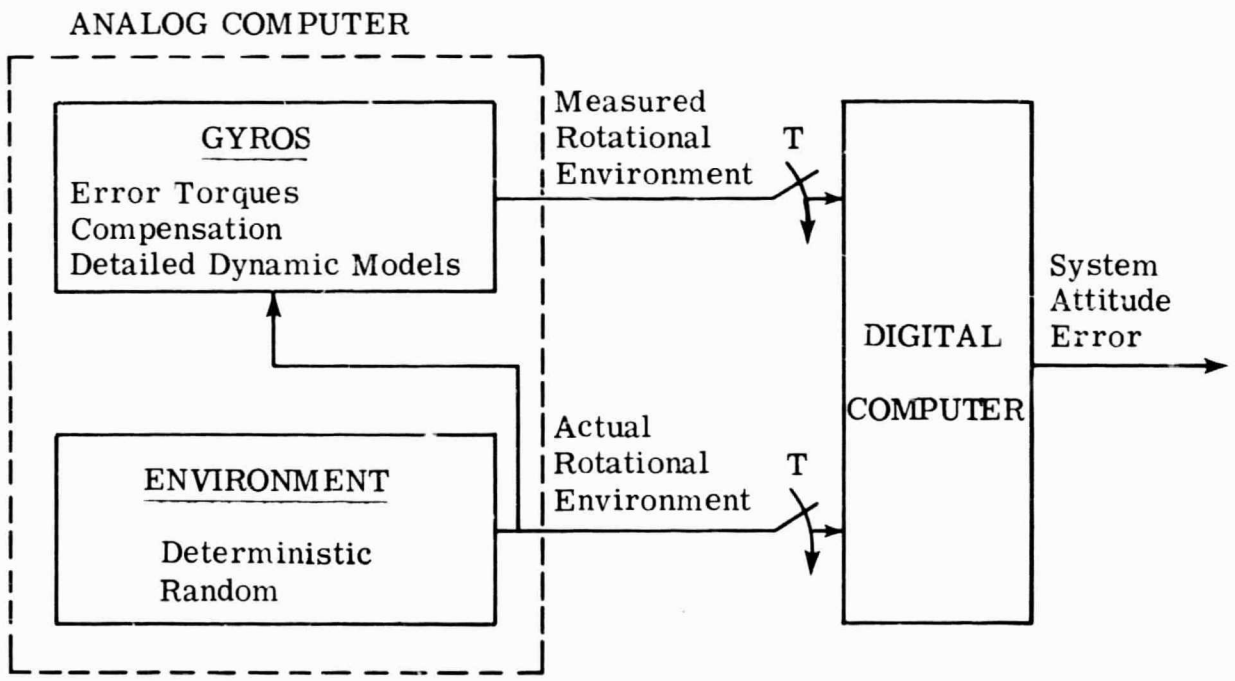

Figure 5.1-1 Hybrid Simulation of Gyros and Calculation of System Attitude Error

5.2 PROGRAM FOR THE DIGITAL PORTION

One function of an inertial navigation system is to provide an indication of vehicle orientation with respect to a reference coordinate frame. In strapdown systems this requirement is satisfied by computing a direction cosine matrix, C, relating vehicle and navigation reference frames. Given an initial C matrix, the direction cosines can be computed from the history of rotations about each body axis. If we compute C at discrete intervals T seconds apart, the direction cosines at the end of the (n + 1)st interval can be expressed in terms of those at the end of the prior period and a matrix of incremental angles, $\Delta\theta$ (see Ref. 1). The matrix $\Delta\theta$ contains the angles through which the body axes have rotated since the last sample time. The equation relating the two direction cosine matrices is:

$$C_{n+1} = C_n e^{\Delta\theta_n}. \tag{5.2-1}$$

when computer considerations such as quantization, word length and truncation are ignored. $\Delta\theta_n$ is defined by

$$\Delta\theta_n \triangleq \int_{nT}^{(n+1)T} \begin{bmatrix} 0 & -\omega_z & \omega_y \\ \omega_z & 0 & -\omega_x \\ -\omega_y & \omega_x & 0 \end{bmatrix} dt \tag{5.2-2}$$

where ω_x, ω_y and ω_z are the angular rates about the body axis. In practice the elements of $\Delta\theta_n$ are measured by the x, y and z axis gyros.

Generally, there is a difference between the actual $\Delta\theta_n$ matrix and that obtained from gyro measurements. The difference between the actual $\Delta\theta_n$ matrix and that given by the gyros is a third matrix, E_n, which represents

the error. The presence of E_n results in an error, ΔC, in the C matrix computed from the gyro measurements. Given E_n for all values of n, we can compute ΔC at the end of each interval. A difference equation for ΔC which retains second order small matrices is obtained from the series expansion of Eq. (5.2-1):

$$\Delta C_{n+1} \cong C_{n+1}\left(E_n + \frac{1}{2}(E_n)^2\right) + \Delta C_n C_n^T C_{n+1}(I + E_n) \qquad (5.2\text{-}3)$$

The figure-of-merit for gyro performance, p_n, can be computed from ΔC_n (see Ref. 1):

$$p_n \triangleq \frac{1}{2}\ \text{trace}(\Delta C_n^T \Delta C_n) \qquad (5.2\text{-}4)$$

Description of the Program — At each sample time the digital computer portion of the simulation receives the simulated gyro outputs (pulse counts) and true body rotations (actual $\Delta\theta_n$ matrix) as inputs. The program then proceeds to compute E_n, C_{n+1}, ΔC_{n+1} and p_n. The matrices C_{n+1} and ΔC_{n+1} are stored for the next cycle and p_n is provided as an output. Figure 5.2-1 is a flow chart for the program. On this chart, C_o and ΔC_o are initial condition matrices for C and ΔC, respectively. The number n is the current number of compute cycles executed. This program has been run on a digital computer identical to the one to be used in the simulation. The compute cycle was found to be about 45 msec in duration. This constitutes a lower limit on the size of the sample period T if the digital computer is to process data when received and the analog simulation is not time scaled. The program was also checked out on an IBM QUIK-TRAN time-sharing system. Simulated gyro error inputs in the form of ramps, sinusoids and coning motion were used. In every case the computer program output (p_n) agreed with the expected result. The program is considered ready for use.

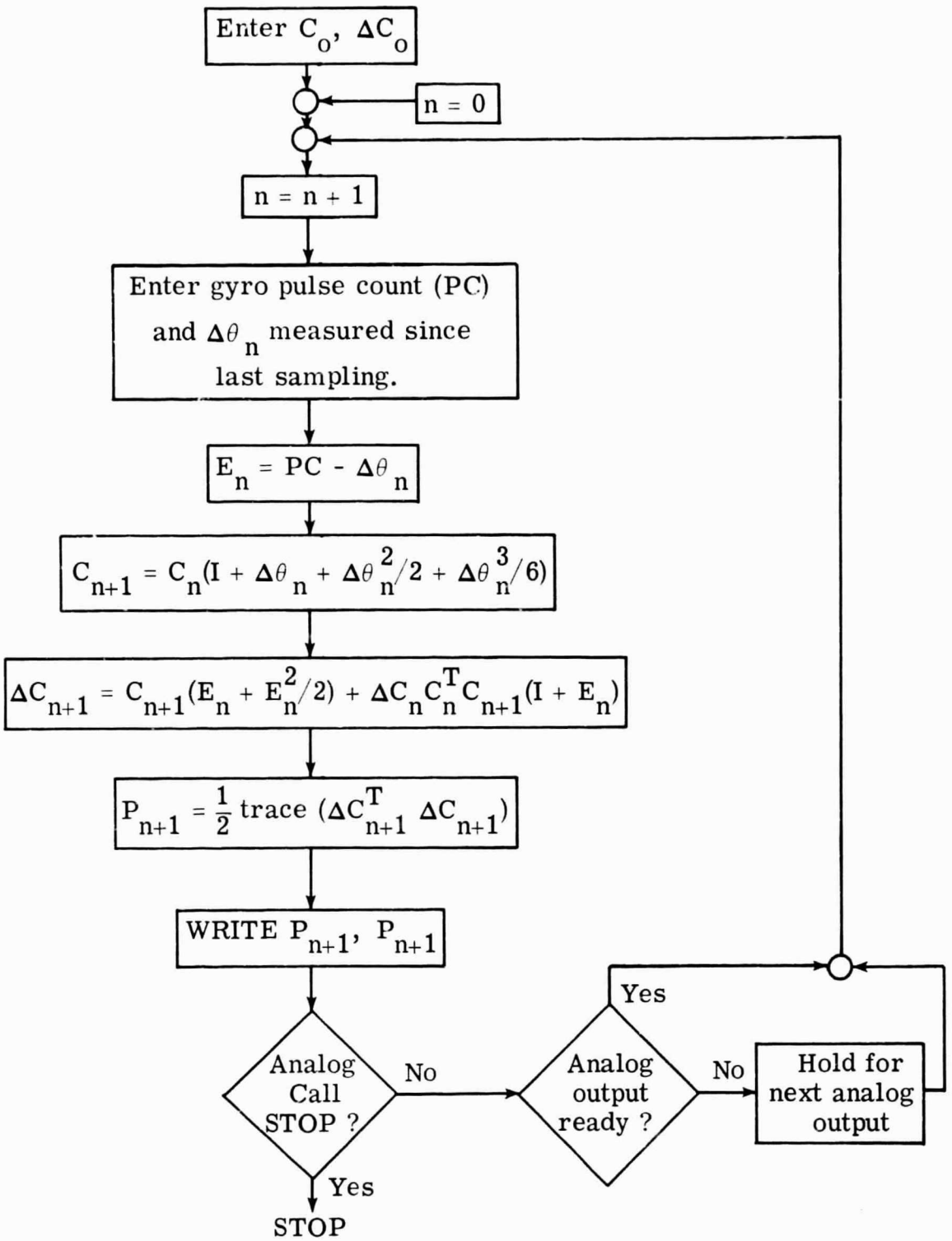

Figure 5.2-1 Flow Chart for the Digital Part of the Hybrid Simulation

6. GIMBAL MISALIGNMENTS CAUSED BY OUTPUT AXIS ANGULAR MOTION

A single-degree-of-freedom gyro experiences torques about its input axis which result from angular rates about its output axis. These torques misalign the float about the input axis, IA, to a degree which depends on the stiffness of the float suspension. Suspension stiffness together with the flotation fluid determine the time constant of the relative motion between case and float. In this section we analyze the time response of the float misalignment about IA to a step angular rate applied about the input axis, OA.

Figure 6.1-1 shows the model assumed for float dynamics about the input axis. The suspension stiffness is represented by linear springs and fluid damping by a pair of dashpots.

α_i = Float-to-case angular misalignment about IA

α_o = Float-to-case angular misalignment about OA

ω_i = Case angular rate about IA

ω_o = Case angular rate about OA

I_{ii} = Float moment of inertia about IA

H = Wheel angular momentum

ℓ = Distance between float center of mass and each float bearing

D = Equivalent linear damping constant in dyne-sec/cm

C_i = Equivalent rotational damping constant in dyne-cm-sec
$= D\ell^2$

K = Equivalent linear spring constant in dyne/cm

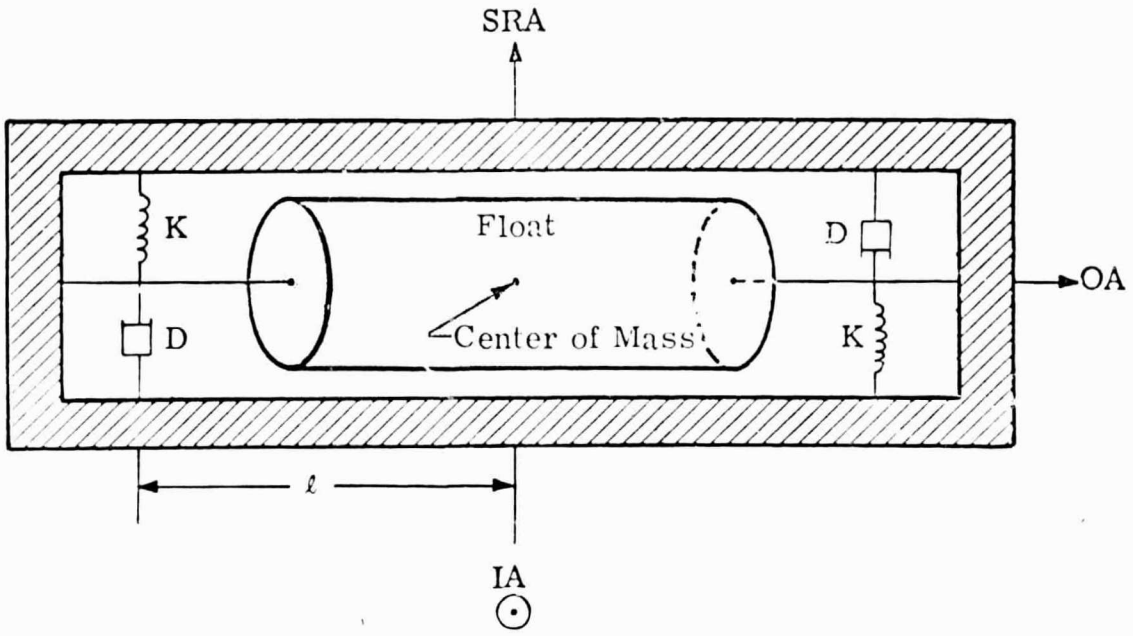

Figure 6.1-1 Model for Gyro Case and Float Dynamics

The equation for angular motion of the float about IA is derived:

Torque on Float = Gyroscopic Torque -
(Spring + Damper Reaction Torques)

$$= I_{ii}(\dot{\omega}_i + \ddot{\alpha}_i)$$

or

$$I_{ii}(\dot{\omega}_i + \ddot{\alpha}_i) = -H(\omega_o + \dot{\alpha}_o) - 2D\ell^2\dot{\alpha}_i - 2K\ell^2\alpha_i \qquad (6.1\text{-}1)$$

Simplifying, we have

$$-\frac{H}{I_{ii}}(\omega_o + \dot{\alpha}_o) - \dot{\omega}_i = \ddot{\alpha}_i + 2\zeta\Omega_n\dot{\alpha}_i + \Omega^2\alpha_i \qquad (6.1\text{-}2)$$

where

$$\zeta = \frac{D\ell}{\sqrt{2KI_{ii}}} \qquad (6.1\text{-}3)$$

$$= \frac{C_i}{\ell\sqrt{2KI_{ii}}}$$

and

$$\Omega_n = \ell\sqrt{\frac{2K}{I_{ii}}} \qquad (6.1\text{-}4)$$

If we assume $\dot{\omega}_i$ and $\dot{\alpha}_o$ to be zero, Eq. (6.1-2) reduces to

$$\ddot{\alpha}_i + 2\zeta\Omega_n\dot{\alpha}_i + \Omega_n^2\alpha_i = -\frac{H}{I_{ii}}\omega_o. \tag{6.1-5}$$

For most gyros the float motion is heavily damped and the response to a step of angular rate about OA can be accurately described by a single time constant, τ:

$$\alpha_i = -\frac{\omega_o}{\Omega_n^2}\left(\frac{H}{I_{ii}}\right)(1 - e^{-t/\tau}) \tag{6.1-6}$$

$$\tau = \frac{1}{\Omega_n(\zeta - \sqrt{\zeta^2 - 1})} \cong \frac{C_i}{K\ell^2} \tag{6.1-7}$$

Equations (6.1-3), (6.1-4), (6.1-6) and (6.1-7) are used to compute float misalignment behavior for different values of C_i and K. The fixed gyro parameters chosen are

$$H = 2.5 \times 10^5 \text{ dyne-cm-sec}$$

$$\ell = 3.6 \text{ cm}$$

$$I_{ii} = 300 \text{ gm-cm}^2$$

Three plots are presented to assist the gyro designer in picking the appropriate suspension stiffness and damping coefficient to constrain misalignment about IA.

Figure 6.1-2 shows the behavior of the float time constant, τ, as a function of K and C_i. Given τ we can enter Fig. 6.1-3 and obtain a time history of the normalized float angle, $2\ell^2 K\alpha_i/H\omega_o$. Note that any time constant

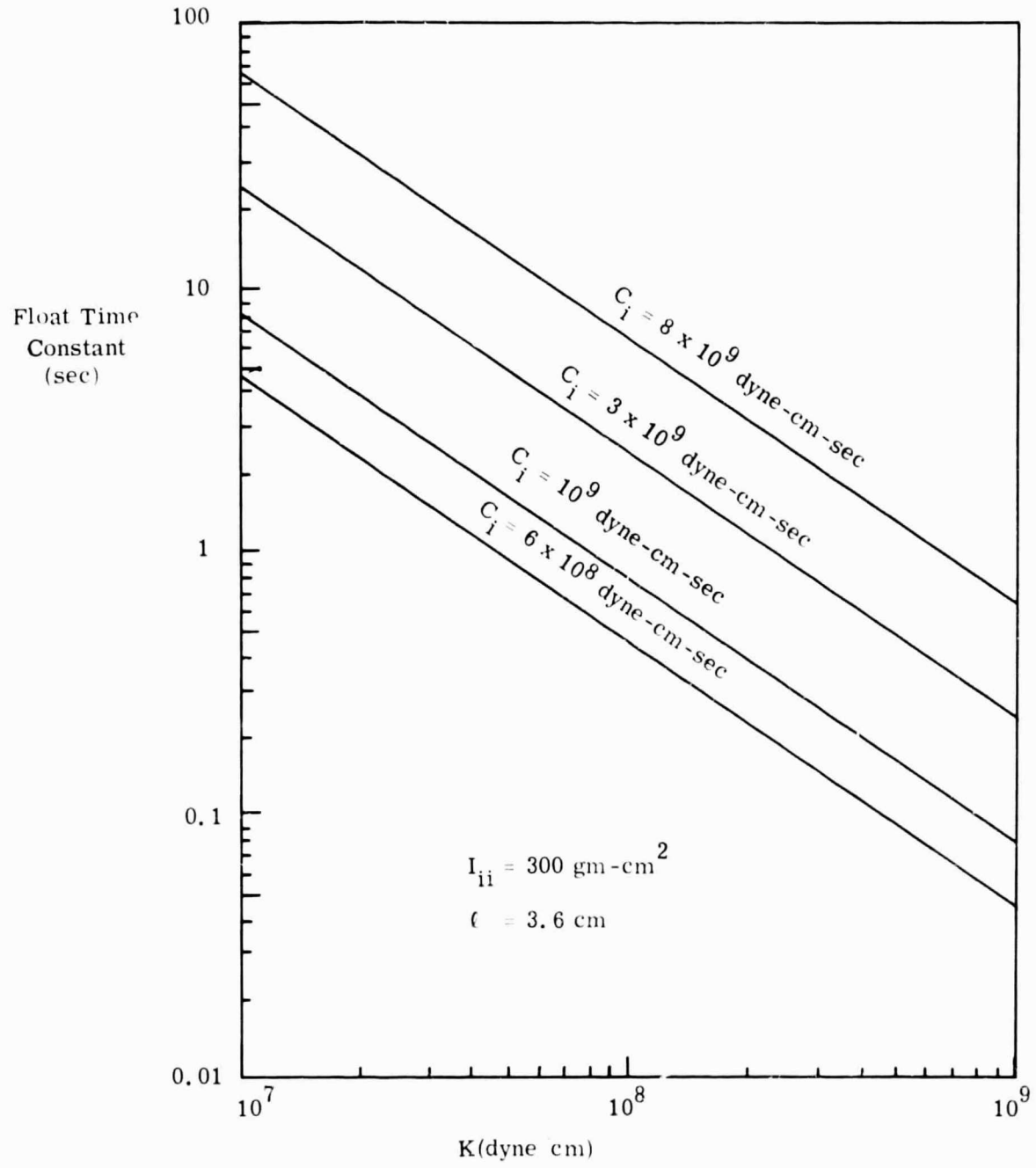

Figure 6.1-2 Float Misalignment Time Constant as a Function of Suspension Stiffness K and Damping Constant C_i.

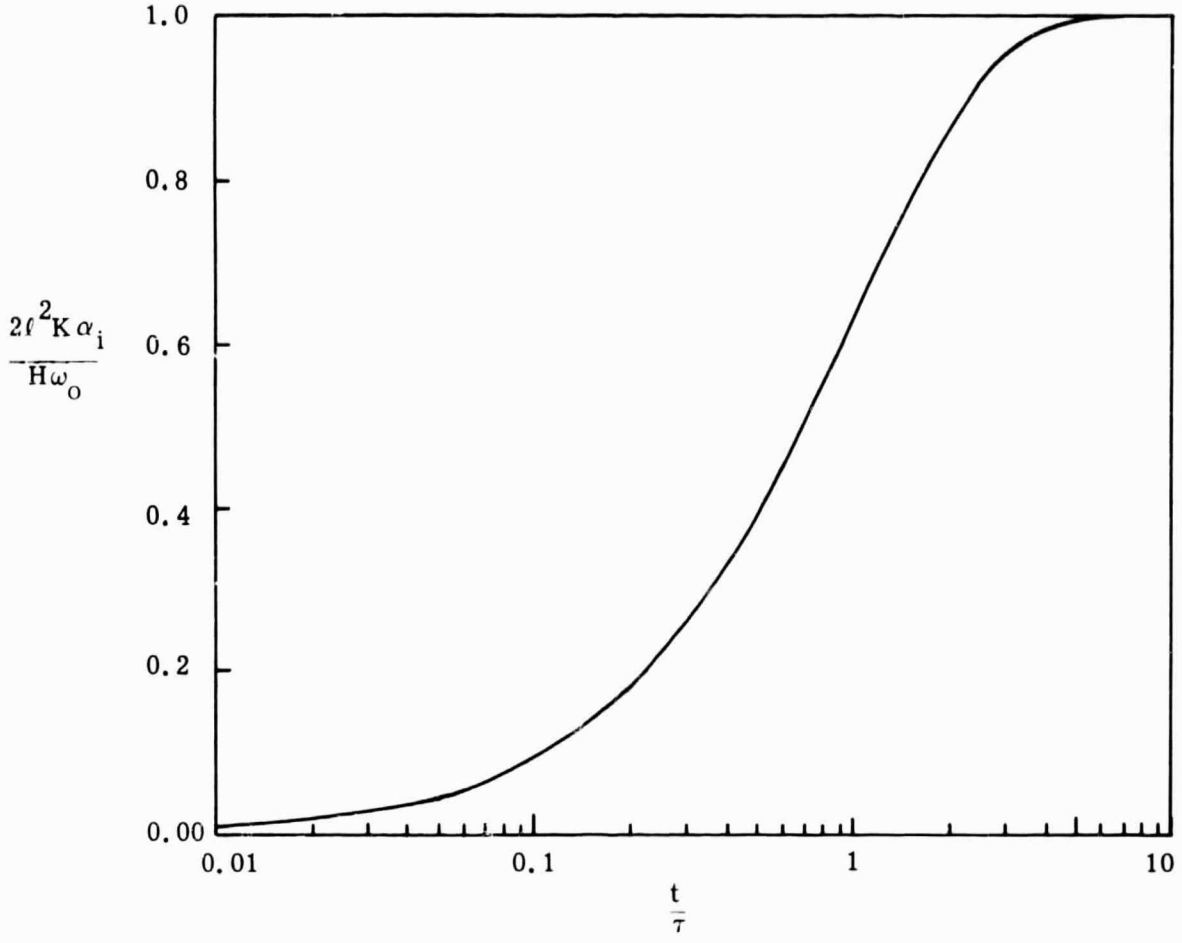

Figure 6.1-3 Normalized Misalignment Angle Response to a Step Angular Rate About the Gyro Output Axis

obtained from Fig. 6.1-2 implies $\ell = 3.6$ cm. Figure 6.1-4 allows us to obtain the misalignment angle as a function of time directly. The effect of suspension stiffness on the time response is readily observed.

If the suspension is not stiff enough for the range of expected output axis rates, the float pivots can strike the bearings. The resulting static friction between pivot and bearing surfaces provides a static break-out torque, τ_s, which masks small torques applied about the output axis by input angular rates. Accordingly, when the three-level torquer is used input rates smaller than τ_s/H are not seen at the sensor loop output, and the gyro has an effective rate dead-zone.

The force, F, pushing each pivot against its bearing results from the gyroscopic torque caused by an output axis angular rate and from forces applied by the gimbal suspension:

$$F = \frac{H\omega_o}{2\ell} - Kd$$

where d is the clearance between bearing and pivot. Knowing μ_{static}, an effective measure of static friction at the pivot-bearing interface, we can evaluate τ_s:

$$\tau_s = 2\mu_{static} F$$

$$= \mu_{static} \left(\frac{H\omega_o}{\ell} - 2Kd \right)$$

$$\pm \mu_{static} \left(\frac{\omega_o}{\ell} - \frac{2Kd}{H} \right)$$

In a binary gyro the constant application of torque by the torque generator prevents this deadzone.

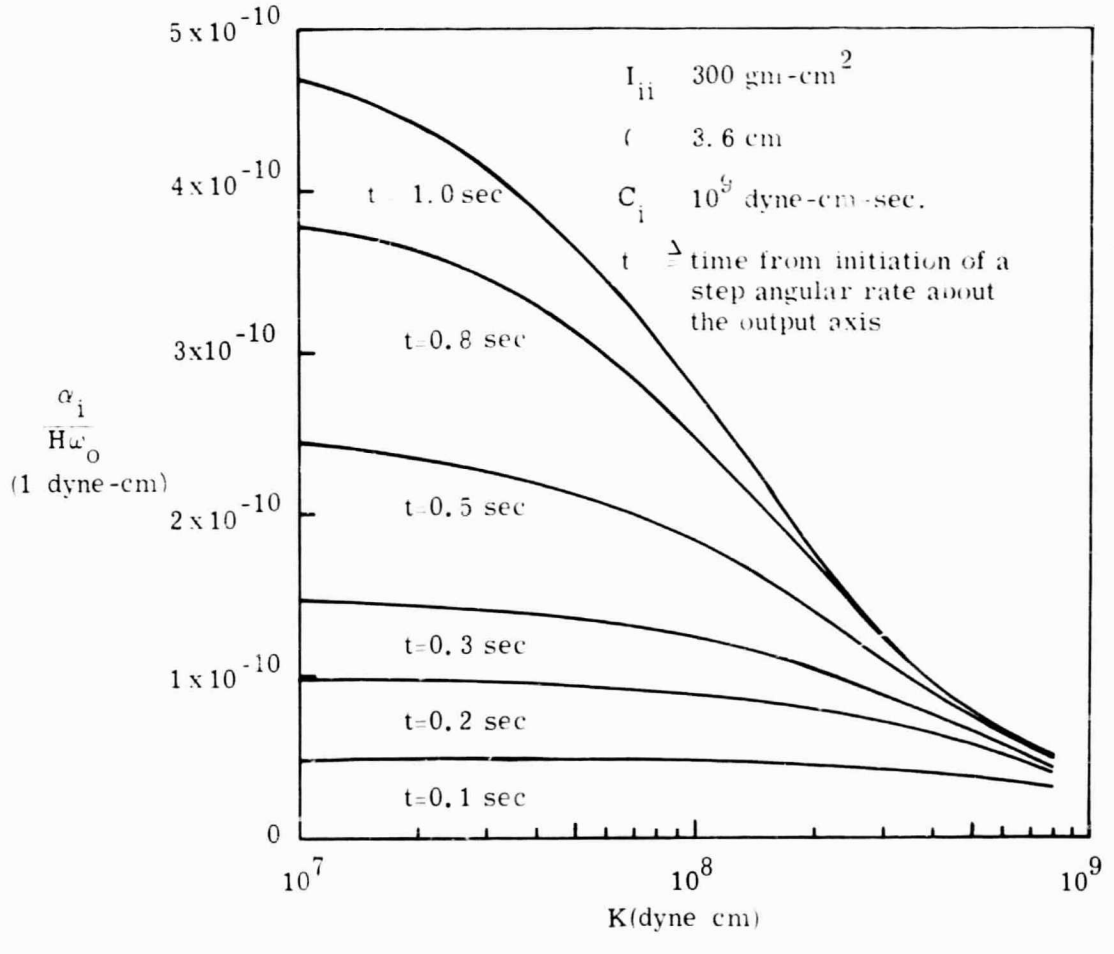

Figure 6.1-4 Normalized Misalignment for Values of Suspension Stiffness

7. CONTINUATION OF EFFORT

Development of the gyro system error simulation will be the focus of future work. For the reasons stated in Sect. 5.1, the hybrid simulation is both a useful and necessary design tool. Upon completion of all the program subsystems presently anticipated, the simulation will first be exercised to check the validity of assumptions used in previous analysis. Then, the possibility of compensating environment-induced gyro errors by processing outputs from the basic sensor triad will be explored. The use of additional angular motion sensors will also be investigated.

The equations for single-of-degree-of-freedom pendulous accelerometer will be developed and compensation for this instrument will be treated by both analysis and simulation.

In brief, it is expected that the remainder of this study will advance knowledge of strapdown sensor errors and their reduction to the point where it can be used as the basis for some hardware construction decisions.

REFERENCES

1. Gelb, Arthur, and Sutherland, Arthur A., Jr., Design of Strapdown Gyroscopes for a Dynamic Environment, Interim Scientific Report, The Analytic Sciences Corporation, TR-101-2, 15 January 1968.

2. Gelb, Arthur, and Sutherland, Arthur A., Jr., Design of Strapdown Gyroscopes for a Dynamic Environment, Semi-Annual Report, The Analytic Sciences Corporation, TR-101-1, 7 July 1967.

3. Gelb, A., and Vander Velde, W. E., Multiple-Input Describing Functions and Nonlinear System Design, McGraw-Hill Book Co., Inc., August 1968.

APPENDIX A

ACCURACY OF THE SMALL SIGNAL APPROXIMATION TO THE DUAL INPUT DESCRIBING FUNCTION FOR THE BINARY NONLINEARITY

In Sect. 3.1 the Dual Input Describing Function (DIDF) gain of the binary nonlinearity is used. The describing function gain for a small signal sinusoid in the presence of a large limit cycle sinusoid is expressed by the approximation:

$$N_B \cong \frac{2D}{\pi A}$$

where A is the limit cycle amplitude at the nonlinearity input and D is the relay drive (output) level. It is desireable to evaluate the accuracy of this approximation.

The DIDF is given for two sinusoids in Appendix D of Ref. 3. Denoting the amplitude of the small signal as B, where $B/A \triangleq \rho$, $\rho < 1$:

$$N_B(A, B) = \frac{8D}{\pi^2 B\rho}\left[E(\rho) - (1-\rho^2)\, K(\rho)\right]$$

where

$$K(\rho) = \int_0^{\pi/2} \frac{d\psi}{\sqrt{1 - \rho^2 \sin^2\psi}} \qquad \text{(Elliptic Integral of the First Kind)}$$

$$E(\rho) = \int_0^{\pi/2} \sqrt{1-\rho^2 \sin^2\psi}\, d\psi \qquad \text{(Elliptic Integral of the Second Kind)}$$

The percentage error in the DIDF estimate caused by using the approximation is

$$\% \text{ Error} = \left\{ \frac{\text{Approximate Value of } N_B}{\text{Exact Value of } N_B} - 1 \right\} \times 100$$

$$= 25 \left\{ \frac{\pi\rho^2 - 4\left[E(\rho) - (1-\rho^2)K(\rho)\right]}{E(\rho) - (1-\rho^2)K(\rho)} \right\}$$

Note that this error is a function of ρ only. Figure A.1 shows the percentage error plotted as a function of ρ. As expected, the error in the approximation goes to zero as the amplitude ratio ρ vanishes.

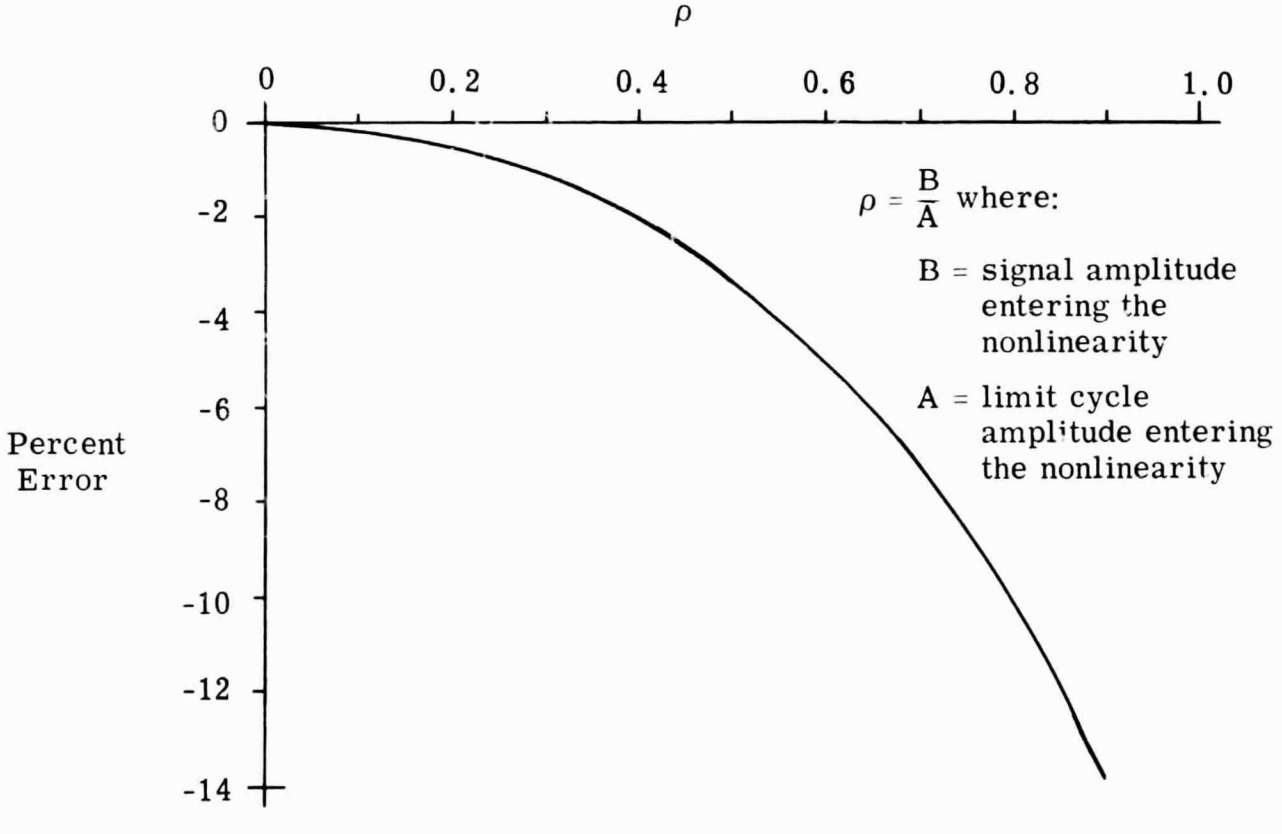

Figure A-1 Error in the Approximation to the DIDF

APPENDIX B

DERIVATION OF THE ELLIPSES USED IN DETERMINING THE FREQUENCY RESPONSE OF THE TERNARY GYRO LOOP

In analysis of the ternary pulse rebalanced gyro loop (see Sect. 4), a graphical solution is used. This is done by using two separate descriptions for the amplitude ratio for a sinusoid on either side of the nonlinear element. One description, developed from linear analysis techniques, generates a family of ellipses. The equation for these ellipses is derived below.

Figure B-1 shows a generalized loop containing a single nonlinearity. N is an equivalent sinusoidal gain (describing function gain) for the nonlinearity and is assumed to involve no phase shift. The loop is driven by a sinusoid of constant amplitude, M, and frequency, ω. The amplitude of the transfer function between the signals A $\sin(\omega t + \phi)$ and M $\sin \omega t$ is:

$$\frac{A}{M} = \left| \frac{\rho_1 e^{j\theta_1}}{1 + N\rho_1\rho_2 e^{j(\theta_1+\theta_2)}} \right| \qquad \text{(B-1)}$$

Using the identity

$$e^{j\theta} = \cos\theta + j\sin\theta \qquad \text{(B-2)}$$

Eq. (B-1) may be written as:

$$\frac{A}{M} = \frac{\rho_1}{\sqrt{(1+N\rho_1\rho_2\cos(\theta_1+\theta_2))^2 + N^2\rho_1\rho_2\sin^2(\theta_1+\theta_2)}} \qquad \text{(B-3)}$$

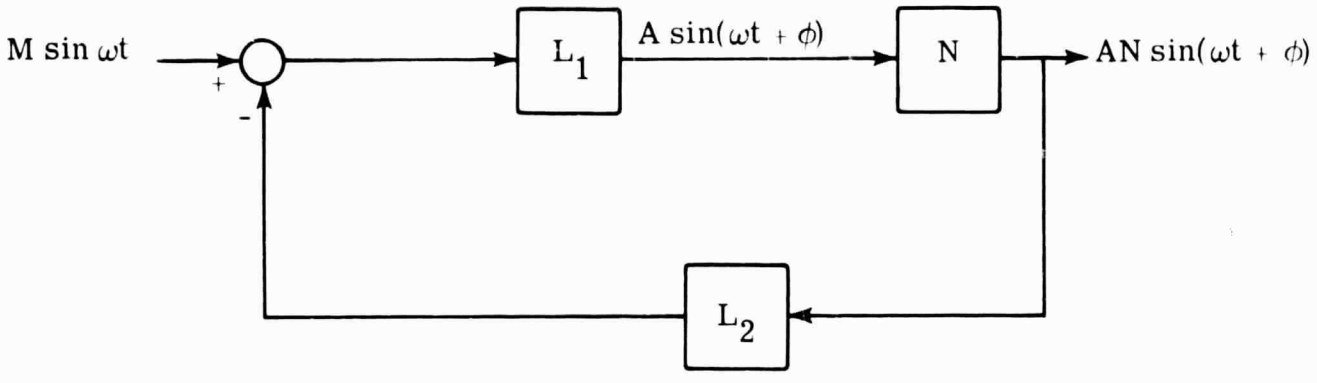

$$L_1 \triangleq \rho_1 e^{j\theta_1}$$

$$L_2 \triangleq \rho_2 e^{j\theta_2}$$

N = equivalent sinusoidal gain of the nonlinearity

Figure B-1 A Loop Containing One Nonlinear Element

Squaring and cross multiplying gives:

$$A^2(1+N\rho_1\rho_2\cos(\theta_1+\theta_2))^2 + A^2N^2\rho_1^2\rho_2^2\sin^2(\theta_1+\theta_2) = M^2\rho_1^2, \qquad \text{(B-4)}$$

Solving for the loop output amplitude, AN, we obtain

$$AN = \frac{-A\cos(\theta_1+\theta_2)}{\rho_1\rho_2} \pm \frac{1}{\rho_1\rho_2}\sqrt{M^2\rho_1^2 - A^2\sin^2(\theta_1+\theta_2)} \qquad \text{(B-5)}$$

In this expression M is given and $\theta_1, \rho_1, \theta_2, \rho_2$ are determined from the frequency ω. Thus, for fixed input amplitude and frequency we have a relation giving the amplitude of the nonlinearity output as a function of A, the amplitude

of its input. Note that AN is independent of the value of N. Plotting AN for values of A yields the ellipse shown in Fig. B-2. Critical points in the construction are illustrated.

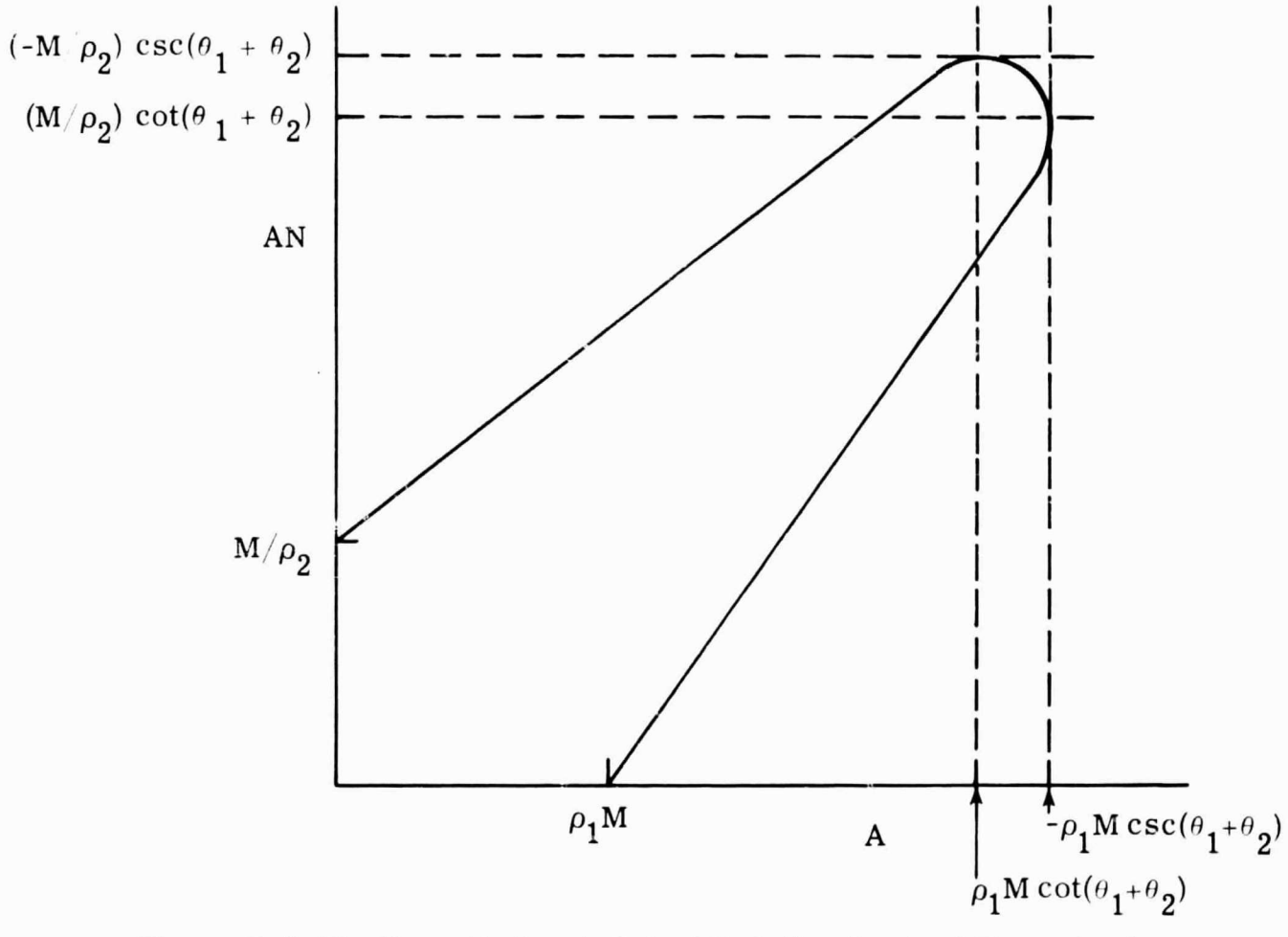

Figure B-2 Nonlinearity Input-Output Relation Derived From Analysis of the Linear Portion of the Loop Shown in Figure B-1